J. Fluid Mech. (2010), *vol.* 655, *pp.* 72–104.
doi:10.1017/S0022112010000662

Generation of secondary droplets in coalescence of a drop at a liquid–liquid interface

B. RAY[1], G. BISWAS[1]† AND A. SHARMA[2]

[1]Department of Mechanical Engineering, Indian Institute of Technology Kanpur, Kanpur 208016, India
[2]Department of Chemical Engineering, Indian Institute of Technology Kanpur, Kanpur 208016, India

(Received 11 April 2009; revised 1 February 2010; accepted 2 February 2010;
first published online 12 May 2010)

When a droplet of liquid 1 falls through liquid 2 to eventually hit the liquid 2–liquid 1 interface, its initial impact on the interface can produce daughter droplets of liquid 1. In some cases, a partial coalescence cascade governed by self-similar capillary-inertial dynamics is observed, where the fall of the secondary droplets in turn continues to produce further daughter droplets. Results show that inertia and interfacial surface tension forces largely govern the process of partial coalescence. The partial coalescence is suppressed by the viscous force when Ohnesorge number is below a critical value and also by gravity force when Bond number exceeds a critical value. Generation of secondary drop is observed for systems of lower Ohnesorge number for liquid 1, lower and intermediate Ohnesorge number for liquid 2 and for low and intermediate values of Bond number. Whenever the horizontal momentum in the liquid column is more than the vertical momentum, secondary drop is formed. A transition regime from partial to complete coalescence is obtained when the neck radius oscillates twice. In this regime, the main body of the column can be fitted to power-law scaling model within a specific time range. We investigated the conditions and the outcome of these coalescence events based on numerical simulations using a coupled level set and volume of fluid method (CLSVOF).

1. Introduction

Various studies have been conducted on the impact of droplets with fluid–fluid interfaces. The behaviours of these impacts can be categorized into the following regimes: splashing (Rein 1996; Morton, Rudman & Liow 2000; Liow 2001; Fedorchenko & Wang 2004), bouncing (Jayaratne & Mason 1964; Ching, Golay & Johnson 1984) and coalescence (Marucci 1969; Cai 1989). Rein (1996) studied the boundaries between splashing and coalescence based on the Weber number, $We = \rho U^2 R/\sigma$, and Froude number, $Fr = U^2/gR$, of the impacting drops, where ρ is the density, U is the velocity of the drop, R is the drop radius, σ is the interfacial surface tension and g is the gravity. This seminal work showed that as the impact velocity of the drop increases, the Weber number and the Froude number increase simultaneously and the coalescence regime shifts towards the splashing regime. Further investigations showed that in the low-velocity regime sometimes the droplet does not coalesce entirely with the underlying liquid layer but a new droplet is pinched off at its top. This phenomenon is called partial coalescence and it produces

† Email address for correspondence: gtm@iitk.ac.in

secondary drops of smaller radius. Partial coalescence is a component of a myriad of complex phenomena such as the droplets in clouds (Berry & Reinhardt 1974), ocean mist and airborne salt particles (Raes *et al.* 2000), emulsions (Bhakta & Ruckenstein 1997) and the generation of vortices near an interface (Thompson & Newall 1885; Sarpkaya 1996). Many exciting studies involving drop/drop coalescence are also available in literature (Menchaca-Rocha *et al.* 2001; Thoroddsen, Takehara & Etoh 2005). In a recent paper, Zhang, Li & Thoroddsen (2009) has experimentally shown the formation of satellite drop during coalescence of two drops similar to the partial coalescence phenomena in the case of drop impact on interface.

The partial coalescence of droplets on a flat air–liquid interface has revealed spectacular features. Schotland (1960) observed that partial coalescence required a low impact velocity of the drop on the interface. Experimental work by Thoroddsen & Takehara (2000) and the numerical model of Pikhitsa & Tsargorodskaya (2000) suggested that the existence of a monolayer surfactant film is crucial for multistage coalescence of a droplet on an air–liquid interface which causes a hole in the intervening air film between the droplet and the underlying liquid. Later, many experimental studies have shown that multistage coalescence can occur even without the presence of surfactants. For fluids of low viscosity, Honey & Kavehpour (2006) identified a narrow intermediate range of drop diameters for which the viscous and gravity forces are both negligible. They had observed up to six secondary drops in which the drop size is reduced by the same fraction in each cycle of partial coalescence and concluded that cascade formation stops due to viscous effects in the case of smaller drops. Honey & Kavehpour (2006) reported the phenomenon of the coalescence-induced bouncing of droplets at gas–liquid interfaces during the coalescence cascade of liquid drops, which they suggested was due to capillary force at the pinch-off.

The first successful experimental work on partial coalescence of liquid drops at liquid–liquid interfaces was published by Charles & Mason (1960*a*,*b*). They concluded that the diameter ratio of the secondary to primary droplets varied with the viscosity ratio $\mu^* = \mu_1/\mu_2$, and passed through a maximum near $\mu^* = 1$. According to this study, partial coalescence occurred when $0.02 < \mu^* < 11$. Contradicting this result, Thoroddsen & Takehara (2000) observed partial coalescence for water and ethanol drops in air with $\mu^* \sim 100$. Charles & Mason (1960*b*) and Mohamed-Kassim & Longmire (2003, 2004) described the partial coalescence process as the propagation and focusing of capillary waves followed by Rayleigh instability. Aryafar & Kavehpour (2006) in their experimental work focused on the time scales of the partial coalescence. Chen, Mandre & Feng (2006*a*,*b*) performed experiments on low-viscosity Newtonian fluids and on polymeric liquids. Their experimental results indicated that for partial coalescence to occur, the drop size has to be in a specific range. Within this range they further defined three regimes: gravity regime, inertio-capillary regime and the viscous regime of partial coalescence. Blanchette & Bigioni (2006) argued both experimentally and numerically that partial coalescence was due to the wave convergence on the top of the droplet and was not due to Rayleigh–Plateau instability. In recent experimental work, Gilet *et al.* (2007*a*) has investigated the ratio between the daughter and the mother droplets and the role of capillary waves on partial coalescence criteria.

After the numerical work of Blanchette & Bigioni (2006), a computational study of partial coalescence between a drop and the interface was performed by Yue, Zhou & Feng (2006). They described the numerical simulations of partial coalescence based on a phase-field method. Through parametric study, they established a criterion for

partial coalescence in terms of a maximum Ohnesorge number which applies to a wide range of fluid densities and viscosities provided that the Bond number is small. Their simulations were limited to low Bo values and also the small-scale events such as pinch-off took place more rapidly than in reality due to numerical diffusion. Very recently, Blanchette & Bigioni (2009) conducted numerical and experimental studies on partial coalescence. The surface tension effect was calculated using an axisymmetric version of the front tracking algorithm of Popinet & Zaleski (1999). They considered both gas and liquid as the surrounding fluid. They observed partial coalescence for systems of low viscosity where capillary waves remain sufficiently vigorous to distort the drop significantly. They also studied the coalescence of two drops of different sizes. Yue *et al.* (2006) and Blanchette & Bigioni (2009) did not highlight the mechanism allowing partial coalescence to occur in absence of capillary waves. The transition from partial to complete coalescence was not addressed well. In the present work, we have attempted to simulate numerically the partial coalescence phenomenon using a coupled level set and volume of fluid method (CLSVOF) to elucidate the underlying physics and to solve the numerical challenges faced by the earlier authors.

The volume of fluid (VOF) method of Hirt & Nichols (1981) forms the building block of computations involving two fluids separated by a sharp interface. In this approach, the grid is fixed and the interface is approximated within each cell through which it passes. Hirt & Nichols (1981) represented the interface by a piecewise-constant line in each two-fluid cell, either vertically or horizontally. A significant improvement of the interface representation was achieved by Youngs (1982) by introducing a piecewise-linear method (piecewise-linear interface calculation, PLIC). The method of Youngs was shown to be very robust and efficient, but only of first-order accuracy. An improved version of the phase interface representation [least square volume interface reconstruction algorithm-(LVIRA)] was devised by Puckett *et al.* (1997).

Welch & Wilson (2000) modified the VOF method to simulate two-dimensional boiling flows and their approach was used in subsequent work in simulating film boiling including conjugate heat transfer with a solid wall (Welch & Rachidi 2002, and in simulating film boiling including the temperature dependence of fluid properties near the critical point Agarwal *et al.* 2004). The VOF method satisfies compliance with mass conservation extremely well. The disadvantage of VOF method is that sometimes it is difficult to capture the geometric properties of the complicated interface.

An efficient interface-capturing method, known as the level set (LS) method, was first introduced by Osher & Sethian (1988). The method is capable of computing the geometric properties of highly complicated boundaries without explicitly tracking the interface. In this method, the boundary of a two-fluid interface is modelled as the zero set of a smooth function ϕ defined on the entire physical domain. The boundary is then updated by solving a nonlinear equation of the Hamilton–Jacobi type on the whole domain. The LS method captures the interface very accurately; however, it may lead to violation of mass conservation if improperly implemented. Sethian (1999) developed a special implementation technique for accurate compliance with mass conservation. Another approach to achieve mass conservation is to couple the LS methodology with the VOF method. In the CLSVOF method (Sussman & Puckett 2000), the LS function is used only to compute the geometric properties (normal and curvature) at the interface while the void fraction is advected using the VOF approach. Tomar *et al.* (2005) and Chakraborty *et al.* (2009) extended the

method to simulate bubble growth in water and the dynamics of air bubble from submerged orifice in reduced gravity, respectively.

When a drop of liquid 1 impacts a liquid 1–liquid 2 interface, the impact either generates a daughter/secondary droplet of liquid 1 or the impacting drop is absorbed without engendering a secondary droplet. The first case will be referred to as a partial coalescence and the later as complete coalescence. The present investigation consists of a computational study and identification of various coalescence events, with emphasis on the conditions and mechanisms leading to partial coalescence and generation of secondary droplets upon the initial impact of a drop of liquid 1 on a liquid 1–liquid 2 interface. We explore the critical values of appropriate non-dimensional parameters for which transition from complete to partial coalescence occurs. The proper explanation pertaining to the mechanism of partial coalescence is still a challenge to be solved. Gilet *et al.* (2007*a*) have showed experimentally how the capillary waves affect the outcome of the coalescence. We studied six different cases and tried to get better insights into the mechanism of partial coalescence. An interesting question also addressed in this section is whether the process of coalescence is monotonic or involves oscillations of the coalescing drop before it is engulfed in the bulk phase. We show that this question is intimately related to the transition from partial to complete coalescence. We also investigate the possibility of finding self-similarity of profiles at the onset of complete coalescence regime.

Rest of the paper is arranged as follows: the governing equations and the CLSVOF-based numerical approach to solve them are described in § 2. The steps used in the numerical method are explained in detail. In § 3, our results are validated with previous experimental results. The results of the phenomenon of partial coalescence and the occurrence of complete coalescence are shown and discussed in § 4. A discussion § 5 is added where the criteria for partial coalescence are discussed. Finally, we draw conclusions on the various aspects of the process in § 6.

2. Computational domain and numerical method

Complete numerical simulation of the processes of partial coalescence is performed for a two-dimensional incompressible flow which is described in axisymmetric coordinates (r, z) as shown in figure 1 (*a*, *b*). The rectangular domain has height $H = 7D$ and width $R = 3D$. The depth of the lower bulk liquid is $H_1 = 3D$. The drop is released at $H_2 = 0.1D$ from the flat interface, where D is the initial drop diameter. The drop falls due to gravity force in the z direction. The change in its shape and velocity because of the resistance of the surrounding fluid are included in our computations. In liquid–liquid systems the rupture is mostly off centre as shown by Gilet *et al.* (2007*a*). Charles & Mason (1960*a*) had mentioned about three types of film rupture, in centre, off centre and double rupture. In all the cases as the initial neck extends in all direction, the flow becomes nearly symmetry. Though our assumption of axial symmetry model does not take into account the initial stages of coalescence, but it accurately captures the later stages of the phenomena as shown in our validations in § 3. The drop shape is important in case of gravity-driven motion of the droplet impacting on liquid–liquid interface. In our simulations for high gravitational force deformation of drop and the interface are captured well. The governing equations and the boundary conditions used for this computational domain are described below. An outline of numerical method is also given.

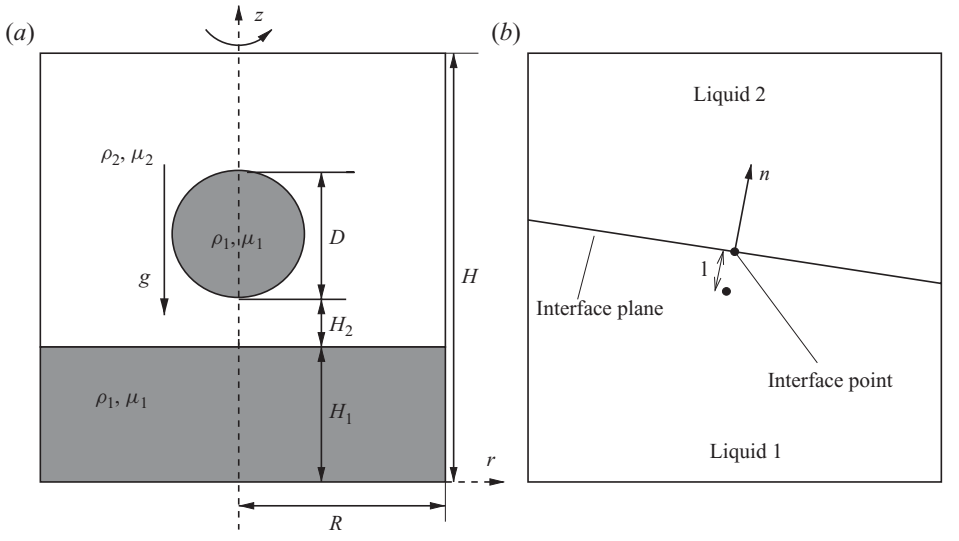

FIGURE 1. (*a*) Computational domain for partial coalescence phenomenon on an (r, z) plane, (*b*) A typical two-phase cell with piecewise linear interface.

2.1. *Governing equations*

The mass and momentum conservation equations for incompressible Newtonian fluids for the liquids 1 and 2 are given by

$$\nabla \cdot \boldsymbol{V} = 0, \tag{2.1}$$

$$\rho\left(\frac{\partial \boldsymbol{V}}{\partial t} + \nabla \cdot \boldsymbol{V}\boldsymbol{V}\right) = -\nabla P + \rho \boldsymbol{g} + \nabla \cdot [\mu(\nabla \boldsymbol{V} + (\nabla \boldsymbol{V})^T)] + f_{sv}, \tag{2.2}$$

where, $\boldsymbol{V}$ is the velocity vector, P is the pressure and f_{sv} is the surface tension force per unit volume.

At the interface, the modified momentum equation incorporating surface tension force due to Brackbill, Kothe & Zemach (1992) becomes

$$\rho\left(\frac{\partial \boldsymbol{V}}{\partial t} + \nabla \cdot \boldsymbol{V}\boldsymbol{V}\right) = -\nabla P + \rho \boldsymbol{g} + \nabla \cdot [\mu(\nabla \boldsymbol{V} + (\nabla \boldsymbol{V})^T)] + \sigma \kappa \boldsymbol{n} \delta_s, \tag{2.3}$$

where σ is the surface tension force, $\boldsymbol{n}$ is the unit normal vector at the interface (figure 1*b*), κ is the mean curvature of the interface and δ_s is the interface delta function.

In the computational domain under consideration, the particular phase (liquid 1 or liquid 2) is defined by the volume fraction F in a control volume as the fraction of the liquid inside a cell as

$$F = (\rho - \rho_2)/(\rho_1 - \rho_2),\ F = \begin{cases} 0 & \text{liquid 2 cell,} \\ 1 & \text{liquid 1 cell,} \\ 0 < F < 1 & \text{interface between liquid 1 and liquid 2.} \end{cases} \tag{2.4}$$

The motion of the moving interface is computed by solving the advection equation for the volume fraction F. The advection equation in its conservative form can be

written as

$$\frac{\partial F}{\partial t} + \nabla \cdot (\boldsymbol{V} F) = 0. \tag{2.5}$$

The CLSVOF method combines the advantages of both the LS and VOF methods. The VOF advection ensures mass conservation and the smoothness of the additionally computed LS function allows the use of simple finite differencing schemes for the calculation of the interface normal vector and the curvature of the interface.

In the LS method, a smooth function ϕ is used to represent the interface. The function $\phi(\boldsymbol{r}, t)$ at a point with position vector $\boldsymbol{r}$ and at a time instant t assumes values as follows:

$$\phi(\boldsymbol{r}, t) \begin{cases} < 0 & \text{in the liquid 2 region,} \\ = 0 & \text{at the interface,} \\ > 0 & \text{in the liquid 1 region.} \end{cases} \tag{2.6}$$

The LS function chosen here is maintained as the signed distance from the interface close to the interface. Hence, near the interface,

$$\phi(\boldsymbol{r}, t) \begin{cases} = -d & \text{in the liquid 2 region,} \\ = 0 & \text{at the interface,} \\ = +d & \text{in the liquid 1 region,} \end{cases} \tag{2.7}$$

where $d = d(\boldsymbol{r})$ is the shortest distance of the interface from point $\boldsymbol{r}$. From such a representation of the interface, the unit normal vector $\boldsymbol{n}$ and the mean curvature κ are simply,

$$\boldsymbol{n} = \frac{\nabla \phi}{|\nabla \phi|} \tag{2.8}$$

and

$$\kappa = -\nabla \cdot \boldsymbol{n} = -\nabla \cdot \frac{\nabla \phi}{|\nabla \phi|} = -\left(\frac{\phi_y^2 \phi_{xx} - 2\phi_x \phi_y \phi_{xy} + \phi_x^2 \phi_{yy}}{\left(\phi_x^2 + \phi_y^2\right)^{3/2}} \right). \tag{2.9}$$

Using the LS formulation due to Chang *et al.* (1996), the momentum equation for incompressible two-phase flow becomes

$$\rho(\phi)\left(\frac{\partial \boldsymbol{V}}{\partial t} + \nabla \cdot \boldsymbol{V}\boldsymbol{V} \right) = -\nabla P + \rho(\phi)\boldsymbol{g} + \nabla \cdot [\mu(\phi)(\nabla \boldsymbol{V} + (\nabla \boldsymbol{V})^T)] + \sigma \kappa(\phi) \nabla H(\phi). \tag{2.10}$$

In this method using the initially known position of the interface (the LS function), the interface is captured by solving the advection for the LS function as

$$\frac{\partial \phi}{\partial t} + \nabla \cdot (\boldsymbol{V}\phi) = 0. \tag{2.11}$$

The density and viscosity are derived from the LS function as

$$\rho(\phi) = \rho_1 H(\phi) + \rho_2 (1 - H(\phi)) \tag{2.12}$$

$$\mu(\phi) = \mu_1 H(\phi) + \mu_2 (1 - H(\phi)) \tag{2.13}$$

where $H(\phi)$ is the Heaviside function,

$$H(\phi) = \begin{cases} 1 & \text{if} \quad \phi > \epsilon, \\ \dfrac{1}{2} + \dfrac{\phi}{2\epsilon} + \dfrac{1}{2\pi} \left\{ \sin\left(\dfrac{\pi \phi}{\epsilon} \right) \right\} & \text{if} \quad |\phi| \leqslant \epsilon, \\ 0 & \text{if} \quad \phi < -\epsilon, \end{cases} \tag{2.14}$$

where ϵ is the interface numerical thickness which we have taken in our simulations as $0.1\Delta r$ (Δr refers to the size of a mesh cell). By using the smoothed Heaviside function, one effectively assigns the interface a fixed finite thickness of a small parameter of the order ϵ, over which the phase properties are interpolated. The details of numerical solutions were well documented by Gerlach *et al.* (2006). The numerical simulations were performed using an in-house code that was tested rigorously for different test cases reported in the literature.

2.2. *Boundary conditions*

Figure 1 (*a*, *b*) shows the domain of interest for the present investigation. The simulation is axisymmetric two-dimensional. At the axis of symmetry ($r = 0$) we set that no fluid exits the domain and the gradient of the velocity must not have a kink:

$$\boldsymbol{V} \cdot \boldsymbol{n} = 0, (\boldsymbol{n} \cdot \nabla \boldsymbol{V}) \times \boldsymbol{n} = 0. \tag{2.15}$$

The sidewall ($r = R$) is considered to be frictionless, therefore the same boundary conditions as at the symmetric axis must hold.

At the bottom wall ($z = 0$) we have the no-slip and impermeability conditions:

$$\boldsymbol{n} \times \boldsymbol{V} = 0, \boldsymbol{V} \cdot \boldsymbol{n} = 0. \tag{2.16}$$

At the outflow ($z = H$) we have natural Neumann conditions:

$$\boldsymbol{n} \cdot \nabla \boldsymbol{V} = 0. \tag{2.17}$$

The conditions for pressure for the whole boundary is

$$\boldsymbol{n} \cdot \nabla P = 0. \tag{2.18}$$

2.3. *Outline of the computational method*

A staggered grid arrangement (Harlow & Welch 1965) is used as the basis for the numerical algorithm. The convective term in the momentum equation (2.3) is discretized by an essentially non-oscillatory (ENO) scheme of second order (Chang *et al.* 1996). All other space derivatives are centred. Suppose the void fraction distribution F^n at time $t^n = n\Delta t$ is known, and the densities and the viscosities at t^n are calculated based on the Heaviside function. The continuity and momentum equations are discretized in time as

$$\nabla \cdot \boldsymbol{V}^{n+1} = 0, \tag{2.19}$$

$$\boldsymbol{V}^{n+1} = \boldsymbol{V}^n + \left(-\nabla \cdot (\boldsymbol{V}^n \boldsymbol{V}^n) + \boldsymbol{g} + \frac{-\nabla P^{n+1} + \nabla \cdot \mu(\phi^n)(\nabla \boldsymbol{V} + (\nabla \boldsymbol{V})^T)^n + \sigma \kappa(\phi^n) \nabla H(\phi^n)}{\rho(\phi^n)}\right) \Delta t. \tag{2.20}$$

The velocity for the new time step is provisionally predicted from the momentum equations. The predicted velocities are subsequently corrected from the discretized continuity equation using the criterion of divergence-free velocity field. The pressure equation is solved by an iterative method based on a preconditioned Bi-conjugate gradient stable method (Bi-CGSTAB) of VanderVorst (1992). Preconditioning is a strategy by which the number of iterations required for convergence is reduced. It involves multiplying the matrix equation throughout by a suitable matrix, so that the modified problem requires a smaller number of iterations than the original problem. A gradient method seeks to minimize the measure of residual by deriving a sequence

of estimates with residuals until the residual is zero, which gives the exact solution. Once the pressure at the new time level has been obtained, the velocity at the new time level is found from the discrete momentum equation. The numerical scheme is based on the explicit time advancement strategy. The solution scheme described above is second order in space and first order in time. Based on the velocity field at the new time step, a coupled second-order conservative operator split advection scheme is used for discretization of (2.5) and (2.11) as described by Rudman (1997). This is done in four steps as follows:

(i) The LS function and void fraction are fluxed across the cell boundaries in one direction.

(ii) The interface is reconstructed using the newly obtained void-fraction field and LS function. In this step, the interface normal vector can be calculated using the LS function in all two-phase cells. The length l (figure 1*b*) is adjusted to match the given void fraction with the reconstructed interface to locate the interface.

(iii) The LS function and void fraction are fluxed across the cell boundaries in the other direction.

(iv) The interface is again reconstructed using the newly obtained void-fraction field and LS function as described step (ii).

The flux directions are swapped after every time iteration. At each time step after finding the updated LS function ϕ^{n+1} and the VOF function, F^{n+1}, the LS function is reinitialized to the exact signed normal distance from the reconstructed interface by coupling the LS function to the volume fraction (Sussman & Puckett 2000).

2.4. *Scaling analysis*

The coalescence behaviour in liquid–liquid system is governed by the interfacial tension, gravity and the viscosity forces in both liquids. The physical parameters which are involved are surface tension σ, densities of the two liquids ρ_1 and ρ_2, viscosities of the two liquids μ_1 and μ_2, acceleration due to gravity g, and the initial drop diameter D. In liquid–liquid system, the densities of the two liquids is represented using mean density, $\rho_m = (\rho_1 + \rho_2)/2$. Thus the seven-dimensional parameters are ρ_m, μ_1, μ_2, σ, g, D and density difference $\rho_c = \rho_1 - \rho_2$. There are three independent fundamental physical quantities- length, mass and time. Using Buckingham π theorem four non-dimensional numbers are obtained, Bond number, $Bo = \rho_c g D^2/\sigma$, the Ohnesorge numbers, $Oh_1 = \mu_1/\sqrt{\rho_m \sigma D}$ and $Oh_2 = \mu_2/\sqrt{\rho_m \sigma D}$ and the Atwood number, $A = \rho_c/2\rho_m$. The length scales are non-dimensionalized using drop diameter D, and the time is scaled by capillary time, $\tau_c = \sqrt{\rho_m D^3/\sigma}$. Thus non-dimensional length and non-dimensional time scales are function, $f(Oh_1, Oh_2, Bo, A)$ of these four non-dimensional numbers.

3. Validation of numerical approach

3.1. *Space and time resolution*

In order to compare our results with others, the experimental results of Chen *et al.* (2006*a*) were chosen, showing a water drop coalescing with an oil–water interface. The oil-based matrix fluid is 20 % polybutene in decane. The dimensional and non-dimensional parameters used here are shown in table 1. To show the grid independent test four different grid sizes are taken: 150×350, 300×700, 375×875 and 450×1050. Table 2 shows different values of secondary drop diameter for different grids. The percentage difference for 150×350 and 300×700 is around 2 %, while for 300×700 and 375×875 grids the difference is around 1 %. For 375×875 and 450×1050, the

Parameter	Values
D	1.1 mm
ρ_1	1000 kg m^{-3}
ρ_2	760 kgm^{-3}
μ_1	0.001 Ns m^{-2}
μ_2	0.002 Ns m^{-2}
σ	0.0297 N m^{-1}
Oh_1	0.0058
Oh_2	0.0117
Bo	0.0958
A	0.136

TABLE 1. Properties of the reference fluid: oil–water system (oil-based matrix fluid is 20 % polybutene in decane).

Grid	Secondary drop diameter (mm)
150×350	0.306
300×700	0.299
375×875	0.296
450×1050	0.296

TABLE 2. Grid independent test for oil–water system (oil-based matrix fluid is 20 % polybutene in decane).

value of secondary drop is same. In our simulations, a grid of 375×875 is taken. We chose the time step as $\Delta t = 10^{-6}$ s for all the simulations. The time step is taken as less than the capillary time, $\Delta t \leqslant 0.5\sqrt{\rho_m(\Delta x)^3/\pi\sigma}$. The capillary time in our study is 1.27×10^{-6} s.

3.2. *Qualitative comparison*

The process of partial coalescence is completed in primarily two stages. When the drop comes in contact with the interface, it floats on the liquid surface for a few seconds. Then slowly the film between the drop and the interface grows thinner and thinner until it ruptures to create a hole. The second stage of the partial coalescence process is the pinch-off of a secondary drop. In figure 2(*a–l*), different interfacial phenomena for partial coalescence are shown and compared with the experiments of Chen *et al.* (2006*a*). As the matrix fluid ruptures, the interface momentarily becomes singular and the contact region expands rapidly. The rupture of the film is due to van der Waals force when the thickness becomes less than 100 nm. This sets off a surface capillary wave propagating up to the drop surface and radially outwards along the initially flat interface. The drop fluid drains into the bulk due to capillary pressure inside the drop and gravity. When the capillary wave reaches the top of the drop, it imparts a vertical velocity to the interface there, thus lifting it upwards. This slight lift can be seen in figure 2(*g*), where the drop crosses the dotted line indicating the initial drop height. A liquid column is formed which gradually becomes thin. At a certain point (figure 2*i*), necking sets at the base of the column and a secondary drop pinches off (figure 2*k*). The numerical results show very good agreement with the experimental results. Figure 3 show the experimental results of Gilet *et al.* (2007*a*) and our simulated profiles. Gilet *et al.* (2007*a*) have mentioned in their experiments that when the liquid 1 drop is very close to the liquid 1–liquid 2 interface, the liquid

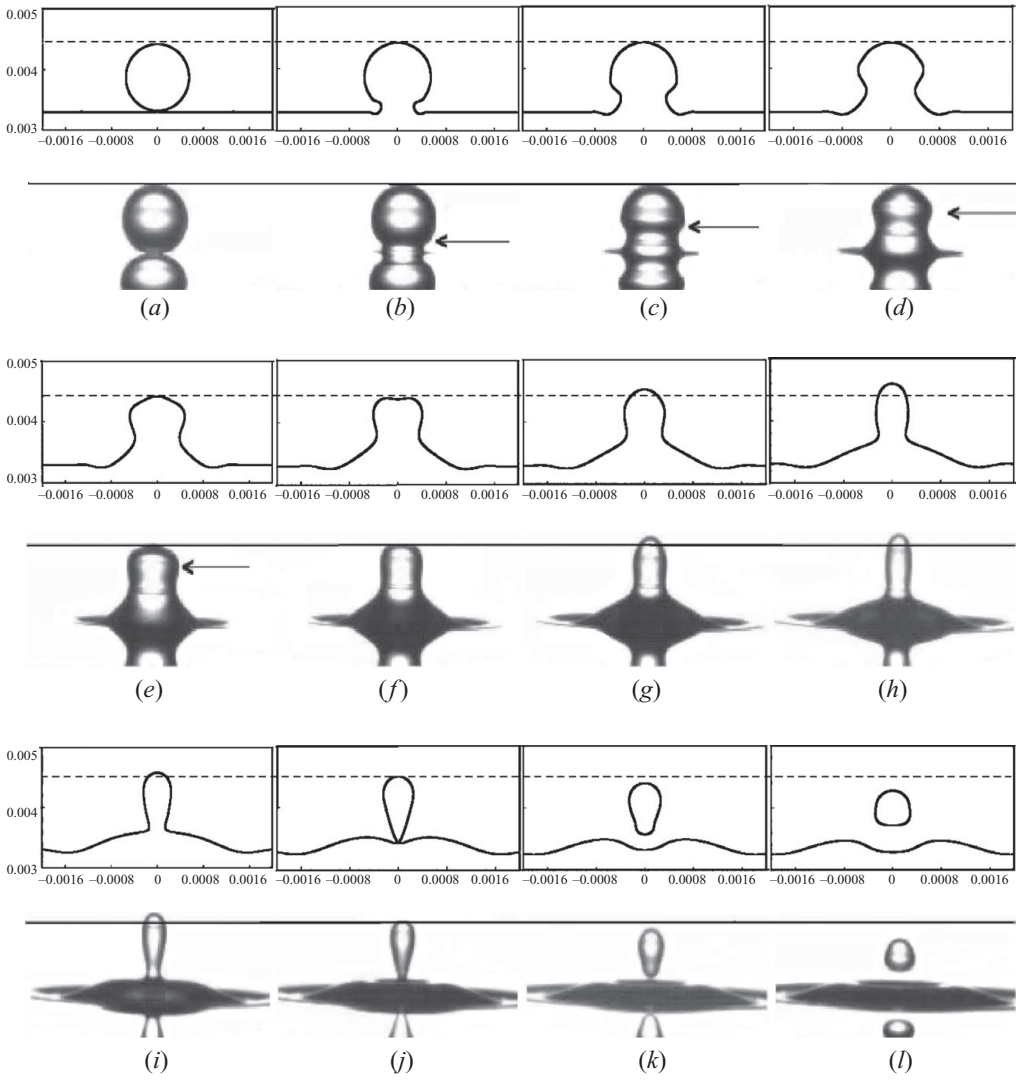

FIGURE 2. Qualitative comparison between present numerical and experimental results of Chen *et al.* (2006*a*) for partial coalescence process with a drop diameter 1.1 mm, $Oh_1 = 0.0058$, $Oh_2 = 0.0117$, $Bo = 0.0958$ and $A = 0.136$. The profiles are 542 μs apart in time. The horizontal line, which are at the same height in all three rows, help in tracking the motion of the top of the drop.

2 film rupture is off centric. Since we have assumed axisymmetric model, we cannot capture the off centric rupture but as shown in figure 3, at further time steps our results show good match with the work of Gilet *et al.* (2007*a*).

3.3. *Quantitative comparison*

Earlier investigations (Aryafar & Kavehpour 2006; Chen *et al.* 2006*a*) mentioned the specific range of diameter for which partial coalescence occurs. Chen *et al.* (2006*a*) have further divided this range into three regions. For small drops, they described the partial coalescence phenomena as being governed by viscous effects. For larger drops, the gravitational effect is the main force. For the medium range of drops, viscous

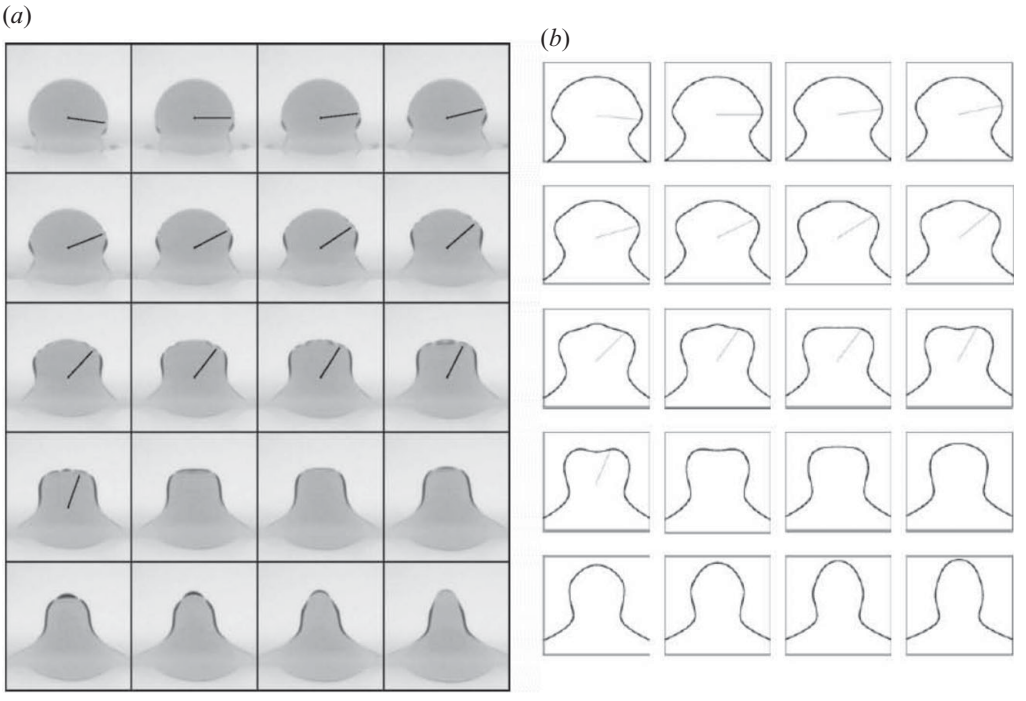

FIGURE 3. Qualitative comparison between experimental results of Gilet *et al.* (2007*a*) (*a*) and present numerical results (*b*) for partial coalescence process with $Oh_1 = 0.002$, $Oh_2 = 0.014$, $Bo = 0.15$. The profiles are $0.045\tau_c$ apart in time.

and gravitational effects are negligible and the inertia and capillary forces become dominant. In this medium range it is observed that the secondary to primary drop ratio, ζ has a nearly constant value of 0.54. Thus the secondary drop formed after partial coalescence is nearly half the size of the initial drop. This region is named the inertio-capillary regime by Chen *et al.* (2006*a*). The process of partial coalescence repeats for the secondary drop in a self-similar manner, as the density of the fluids does not change.

For the other two regimes, the gravity-dominant regime is named the gravity regime and the viscous-dominant regime the viscous regime. In the gravity regime there is a maximum drop diameter (D_U) at which the phenomenon of partial coalescence is not observed. Drops equal to and larger than this particular diameter completely coalesce after impact. After the film has ruptured, the larger drop drains off quickly into the bulk fluid due to more gravity force. Hence the size of secondary drop formed is less than half the size of the primary drop. When the drop size is D_U it is seen that the drainage is so fast that necking no longer occurs, thereby completely coalescing the drop with the bulk fluid. In the other case, for a very small drop, the viscous effect prevents the capillary waves from travelling through the liquid column formed. As the drop size gradually decreases, more resistance to capillary force is created and so gradually the secondary drop size becomes smaller. At a particular diameter D_L, necking formed in the interface cannot be sustained and the drop completely coalesces. This is the minimum diameter below which the partial coalescence phenomenon is not observed.

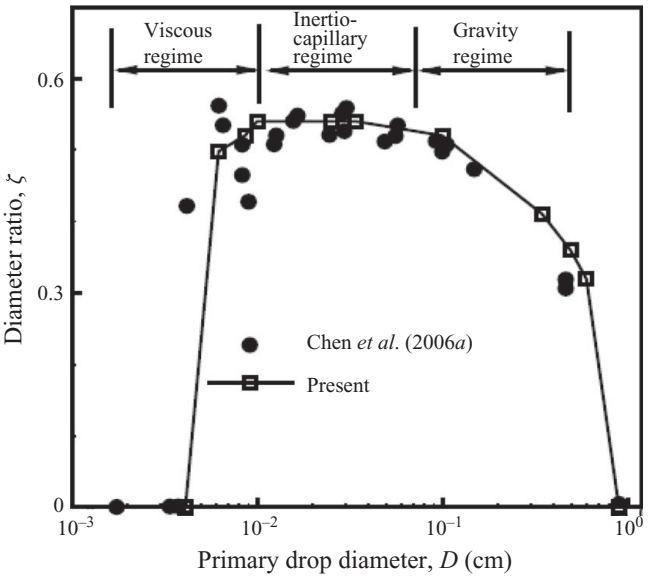

FIGURE 4. (*a*) Quantitative comparison between numerical and experimental results of Chen *et al.* (2006*a*) by plotting the secondary to primary diameter ratio (ζ) versus primary drop diameter (D). The reference fluid is oil–water system (oil-based matrix fluid is 20 % polybutene in decane).

Figure 4 explains this phenomenon clearly. The solid circles represent the experimental results of Chen *et al.* (2006*a*) and the hollow squares are the results obtained in our numerical simulations. According to previous studies (Yue *et al.* 2006), D_L lies between 39 and 78 μm and D_U between 1 and 2 cm. In our simulations, D_L is obtained as 49 μm and D_U as 1.09 cm. Our results shows excellent agreement with the experimental values.

4. Results

4.1. *Coalescence cascade: the self-similar behaviour*

We started our simulation with the dimensionless parameters as $Oh_1 = 0.0058$, $Oh_2 = 0.0117$, $Bo = 0.0958$ and $A = 0.136$. Figure 5 reveals that at $t = 0.75\tau_c$ we observe the first pinch-off. After a few time steps, at $t = 2\tau_c$ we observe a tertiary drop. The diameter ratios in the two steps are 0.54 and 0.47, respectively. The process of partial coalescence completes in a cascade of two steps.

This kind of cascade is described in literature. Honey & Kavehpour (2006) started with a drop diameter of 1.2 mm in water and air system and observed two steps in a cascade with secondary and tertiary drop diameters equal to 0.64 and 0.32 mm, respectively. The drop diameter ratio is nearly the same as ours via the cascade i.e. 0.50 ± 0.05. Furthermore, the process of tertiary drop formation in a liquid–liquid system is slower than that in liquid–air system. The viscosity of the matrix liquid is responsible for this difference. In the inertio-capillary regime, the process of partial coalescence repeats itself in a self-similar fashion (Charles & Mason 1960*b*; Pikhitsa & Tsargorodskaya 2000; Thoroddsen & Takehara 2000). It may be mentioned that Charles & Mason (1960*b*) observed up to eight steps in a cascade by performing experiments for systems of two immiscible liquids. Vandewalle *et al.* (2006) showed a cascade of partial coalescence for soapy water with air as the matrix

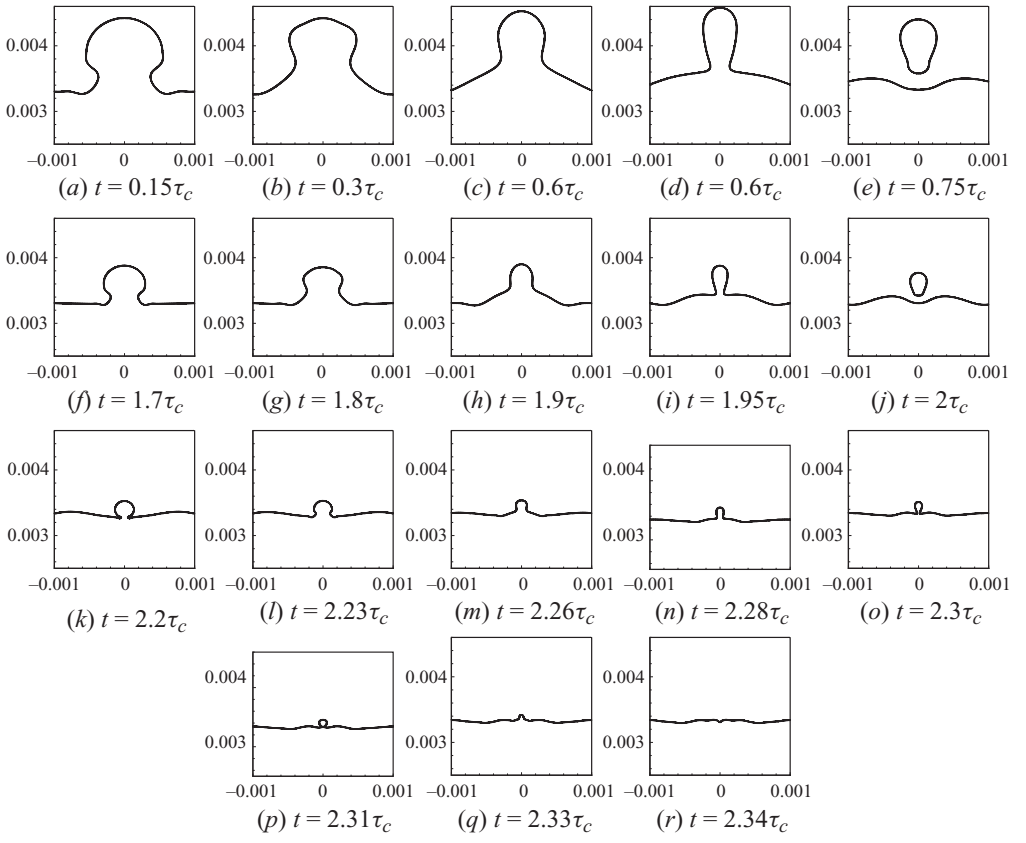

FIGURE 5. Coalescence cascade showing secondary and tertiary drop. The parameters are $Oh_1 = 0.0058$, $Oh_2 = 0.0117$, $Bo = 0.0958$ and $A = 0.136$.

fluid. They observed six successive steps in partial coalescence starting from a 1 mm droplet. Thoroddsen & Takehara (2000) in experiments on liquid (water, alcohol and mercury) and air systems observed up to six steps in a cascade, starting with a drop diameter around 3 mm. When coalescence cascade occurs, the ratio of viscous to surface forces increases as the drop size decreases. The diameter of the drop decreases to a critical diameter and the drop fully coalesces.

Figures 6(*a*) and 6(*b*) describe the shape and motion of the daughter drop, respectively, before it comes to contact with the interface. After the pinch-off, the drop assumes a prolate shape (I) with the drop base close to the liquid–liquid interface. In the figure the liquid–liquid interface depth is defined as the crater depth. In the course of time, the drop slowly moves down and attains an oblate shape (III), and then gradually becomes spherical (X). During this entire time, the crater depth gradually increases and reaches a maximum depth after which the interface again moves up. The interface moves up and the falling drop comes in contact. Subsequently, the second stage of partial coalescence cascade sets in. Similar phenomena are repeated for the tertiary drop.

4.2. *Multiple secondary drops from a parent drop*

Figure 7 shows the formation of two secondary drops of unequal size and their merger. The dimensionless parameters for this simulation are $Oh_1 = 0.0021$, $Oh_2 = 0.0043$,

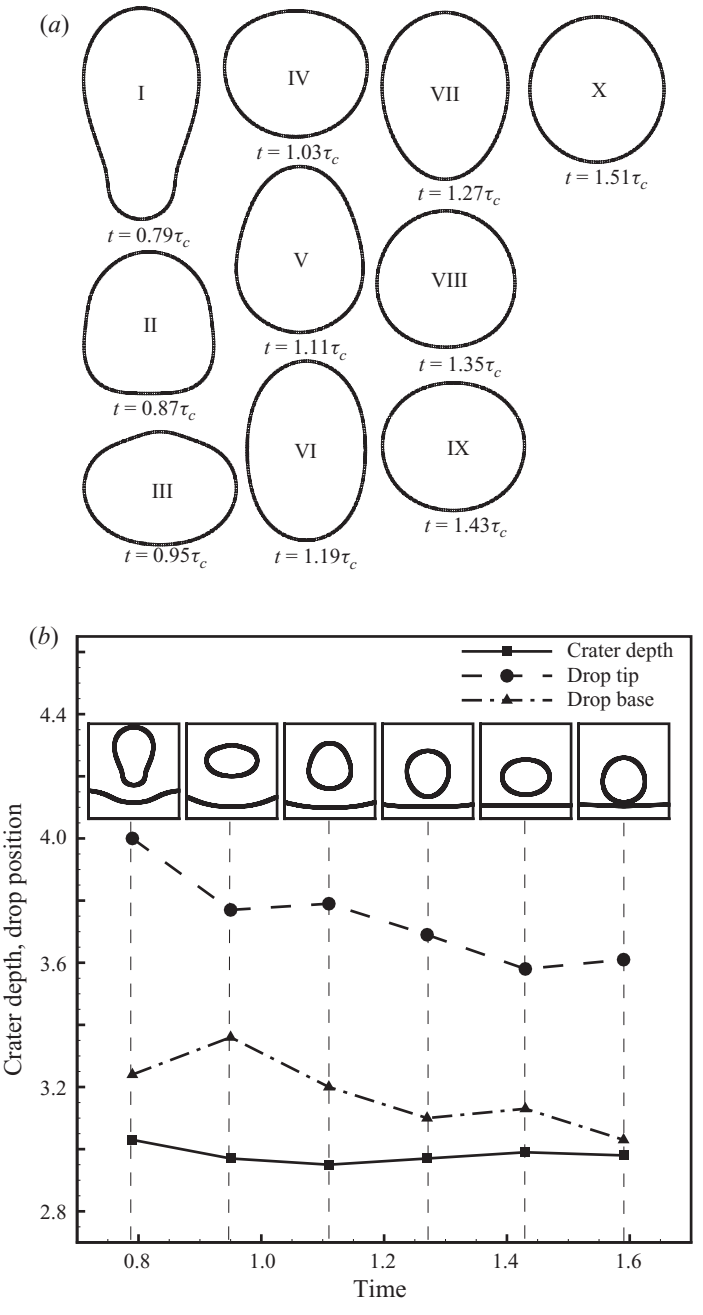

FIGURE 6. (*a*) Shape of the daughter drop. (*b*) Dynamics of secondary and tertiary drop motion. The parameters are $Oh_1 = 0.0058$, $Oh_2 = 0.0117$, $Bo = 0.0958$ and $A = 0.136$.

$Bo = 5.2$ and $A = 0.136$. The process is same as described above until $t = 0.039\tau_c$ when necking occurs at two places, one at the bottom of the column and the other at the middle. This is due to more capillary waves moving up the column. The necking at the middle of the liquid column is due to Rayleigh instability. At $t = 0.04\tau_c$, two secondary drops are formed. These two drops later merge to form

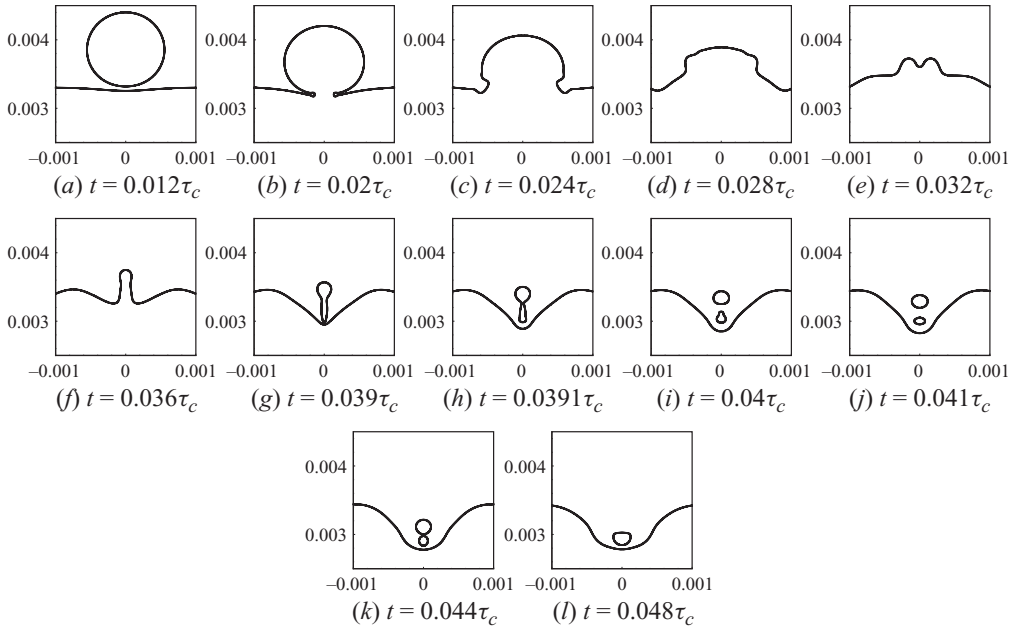

FIGURE 7. Formation of two secondary drops. The parameters are $Oh_1 = 0.0021$, $Oh_2 = 0.0043$, $Bo = 5.2$ and $A = 0.136$.

a single drop. Charles & Mason (1960*b*) had observed that a primary water drop with initial diameter more than 6 mm yields two secondary drops of unequal size when coalescing with a benzene–water interface. Similar pinch-off have been shown by Duchemin *et al.* (2002). There the jet formed after bubble bursting, split into small drops due to Rayleigh Plateau instability.

4.3. *Relative effect of inertia with respect to interfacial tension: the inertio-capillary regime*

The diameter ratio is function of Ohnesorge numbers, Bond number and Atwood number, $d_{secondary}/D = f(Oh_1, Oh_2, Bo, A)$. In figure 8(*a*), the diameter ratio is plotted for various A. Atwood number ranges from $0.136 \leqslant A \leqslant 0.8$. The other parameters are $0.0958 \leqslant Bo \leqslant 0.35$, $0.0058 \leqslant Oh_1 \leqslant 0.0075$ and $0.0117 \leqslant Oh_2 \leqslant 0.014$. The diameter ratio is seen to be nearly constant at 0.54 for the secondary to primary drop ratio, and 0.43 for the tertiary to secondary drop ratio. The time taken starting from the impact of the drop on the interface to the pinch-off of a daughter drop is defined as the pinching time, τ_p. For different A, τ_p values are nearly constant for secondary drops and also for tertiary drops, as shown in figure 8(*b*). Thus the diameter ratio (ζ) and pinching time (τ_p) are seen to be invariant with respect to the Atwood number. In our results the Atwood number shows the asymptotic regime of the function, $f(Oh_1, Oh_2, Bo, A)$. The Atwood number dose not give any correlation with the diameter ratio for this regime. Previously Gilet *et al.* (2007*a*) had also shown such asymptotic regime with the value to be approximately 0.45 for Atwood number less than 20 % and negligible Bo, Oh_1 and Oh_2. Thus, it is actually an asymptotic constant value for different Atwood numbers that characterizes the so called inertio-capillary regime.

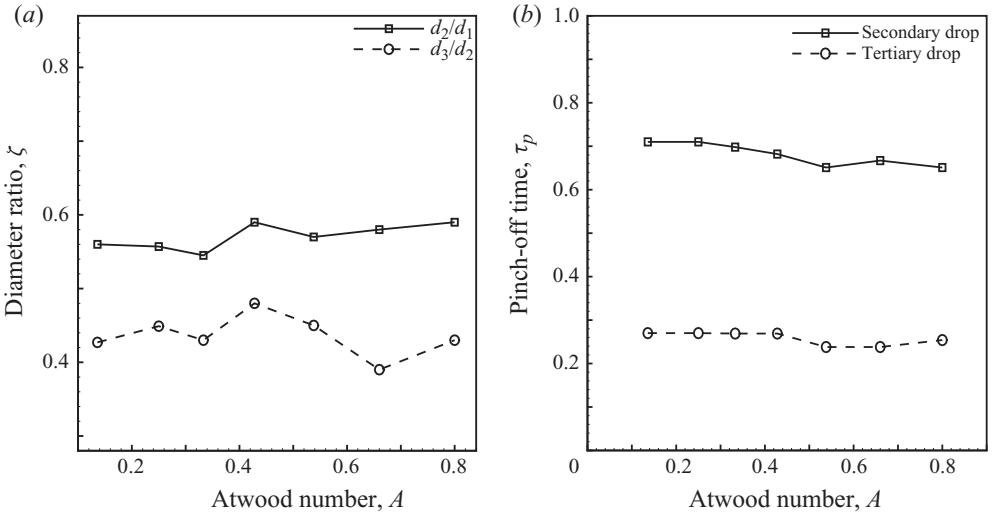

FIGURE 8. (*a*) Diameter ratio (ζ) versus Atwood number (A). d_1, d_2 and d_3 indicate primary, secondary and tertiary drop diameter, respectively. (*b*) Pinch-off time (τ_p) versus Atwood number (A) keeping other parameters at $0.0958 \leqslant Bo \leqslant 0.35$, $0.0058 \leqslant Oh_1 \leqslant 0.0075$ and $0.0117 \leqslant Oh_2 \leqslant 0.014$. Length and time are non-dimensional.

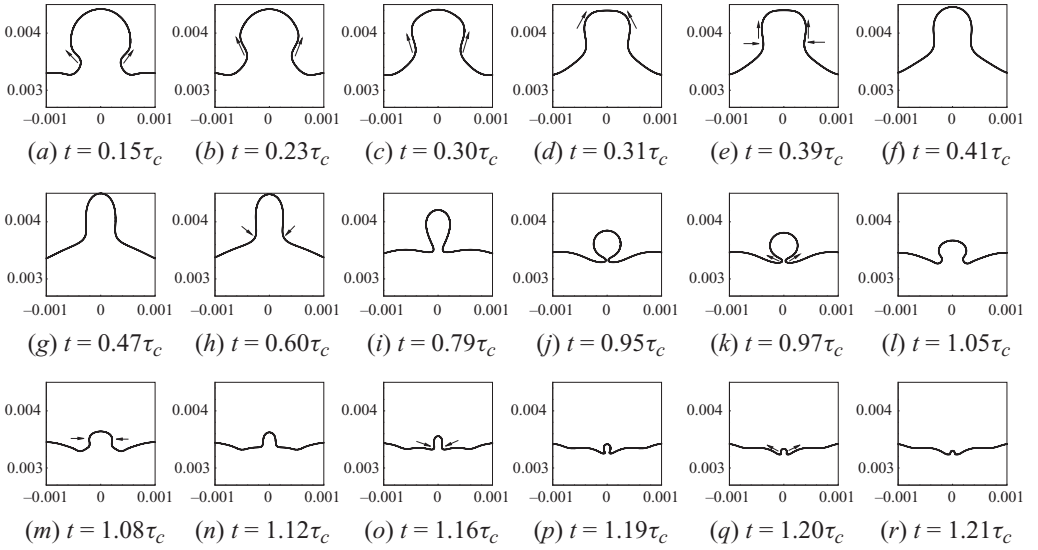

FIGURE 9. Complete coalescence of drop for parameters, $Oh_1 = 0.031$, $Oh_2 = 0.0117 (Oh_1 > Oh_2)$, $Bo = 0.0958$ and $A = 0.136$.

4.4. *Relative effect of viscosity with respect to interfacial tension: the viscous regime*

We have previously mentioned the minimum drop diameter D_L for which partial coalescence is not observed. This corresponds to a maximum Ohnesorge number. Figure 9 shows different steps depicting the complete coalescence of the drop. The non-dimensional parameters for this case are $Oh_1 = 0.031$, $Oh_2 = 0.0117$, $Bo = 0.0958$ and $A = 0.136$. After the film has ruptured, the capillary wave moves towards the drop apex, which is shown by the arrows in the figure up to $t = 0.31\tau_c$. From $t = 0.39\tau_c$

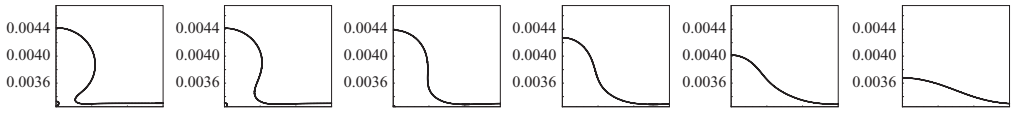

FIGURE 10. Complete coalescence of drop for parameters, $Oh_1 = 0.3$, $Oh_2 = 0.0058 (Oh_1 \gg Oh_2)$, $Bo = 0.0958$ and $A = 0.136$.

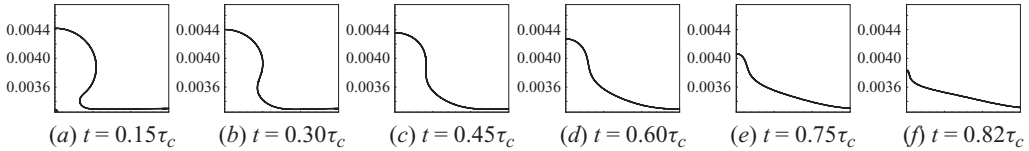

FIGURE 11. Complete coalescence of drop for parameters, $Oh_1 = 0.0058$, $Oh_2 = 0.3 (Oh_2 \gg Oh_1)$, $Bo = 0.0958$ and $A = 0.136$.

to $0.47\tau_c$, a column shape is formed. At $t = 0.6\tau_c$, necking starts and gradually the interface deforms to a spherical shape at $t = 0.95\tau_c$. Due to the high viscous force inside the sphere, the drop starts to drain out into the bulk liquid and pinch-off does not occur. The capillary waves responsible for the pinch-off at the neck are highly damped due to the high viscous effect. From $t = 1.08\tau_c$ to $1.12\tau_c$, again a columnar shape is formed. The necking of this column starts at $t = 1.16\tau_c$, leading to a spherical shape. Finally, the drop completely merges with the bulk liquid.

When the viscosity of liquid 2 is increased by a slight amount ($Oh_2 = 0.1179$), the collapse of the drop takes place in a similar manner. This is explained in detail in § 4.6. For more higher viscosity of the liquid 1 or liquid 2, the drop collapses in a different manner, as shown in figures 10 and 11. In both cases, the drop after coming in contact with the bulk liquid collapses rapidly.

Figure 12(*a*) shows the influence of the Ohnesorge numbers (Oh_1, Oh_2) on ζ for $Bo = 0.0958$ and $A = 0.136$. As Oh_2 increases the diameter ratio decreases smoothly. The critical value for partial coalescence is obtained as $Oh_{2C} \approx 0.12$ (for $Oh_1 = 0.0058$). A totally different trend is observed in the case of increasing Oh_1. Here it is observed that the diameter ratio decreases very sharply. The critical value for the Ohnesorge number is $Oh_{1C} \approx 0.035$ (for $Oh_2 = 0.0058$). The difference between their influences is explained by the viscosities of the two liquids. When the viscosity of the drop is increased while keeping the viscosity of the matrix liquid constant, the capillary wave is gradually damped out. Above a critical viscosity, the drop completely merges. A different phenomenon occurs when the drop viscosity is kept constant and the viscosity of matrix liquid is increased. In this case, the process of emptying of the drop depends on the increasing viscous force applied by the matrix liquid on the drop. Therefore, the change of Ohnesorge numbers shows different trends. The results presented in figure 12(*a*) and the results of figure 4 in Gilet *et al.* (2007*a*) have similar trend of variation of the diameter ratio with Oh_1 and Oh_2.

Figure 12(*b*) shows the variation of pinch-off time (τ_p) as a function of Oh_1. The pinch-off time increases as the viscosity of the drop is increased. As the viscosity of the drop is increased, the capillary waves moving towards the drop apex are damped out. The columnar shape formation takes time and so the necking process is also delayed. When both the viscosities of liquids 1 and 2 are changed, the coalescence

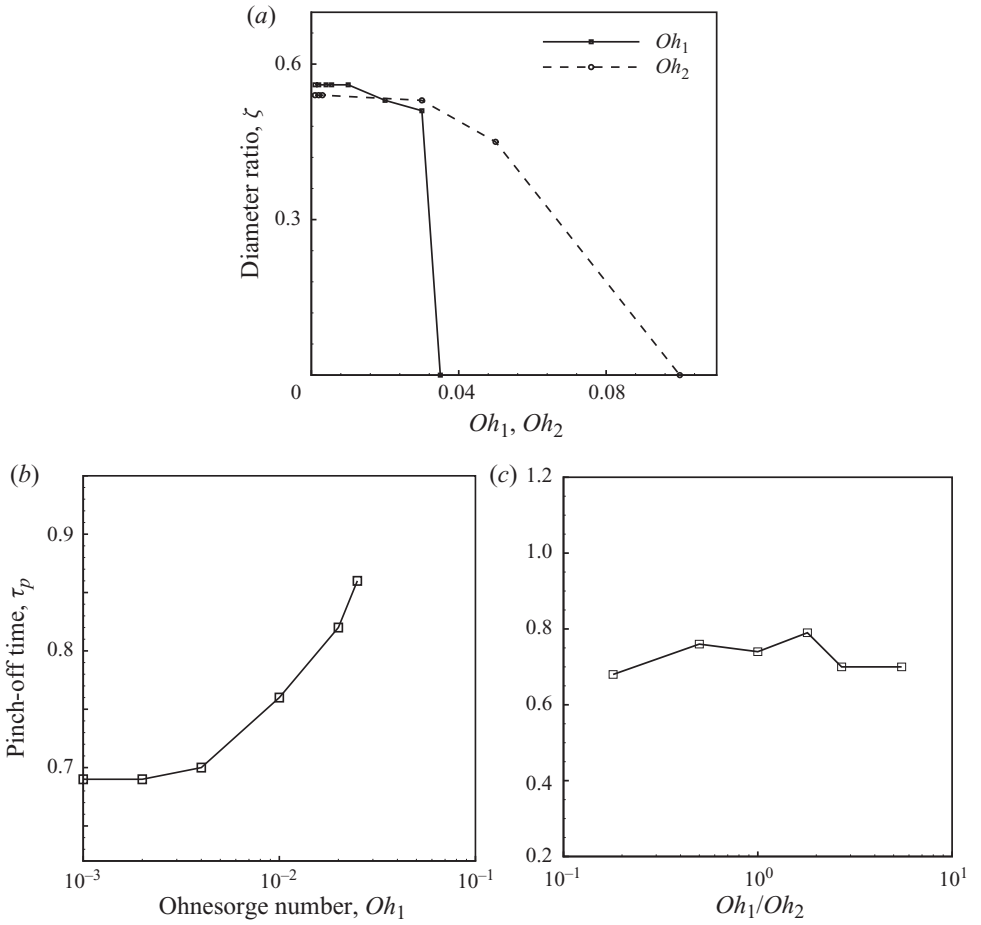

FIGURE 12. (*a*) Diameter ratio (ζ) versus Oh_1 and Oh_2. (*b*) Pinch-off time (τ_p) versus Oh_1. (*c*) Pinch-off time (τ_p) versus Oh_1/Oh_2 with other parameters as $Bo = 0.0958$ and $A = 0.136$. Length and time are non-dimensional.

time is nearly same, as shown in figure 12(*c*). Hence for a viscosity ratio ranging from 0.2 to 6, the process of pinch-off does not vary much.

4.5. *Relative effect of gravity with respect to interfacial tension: the gravity regime*

For a high gravitational force, the value of the Bond number increases. The non-dimensional parameters taken are $Bo = 9.83$, $Oh_1 = 0.0057$, $Oh_2 = 0.114$ and $A = 0.149$. Figure 13 reveals that the thin film below the drop drains out slowly with time, finally creating a hole in the drop when it comes in contact with the interface. Here at $t = 0.30\tau_c$ a small matrix drop, also called satellite drop, is seen to be trapped during film rupture. Such an entrapment was observed by Thoroddsen, Etoh & Takehara (2003) and Chen *et al.* (2006*b*). Chen *et al.* (2006*b*) have used the drop liquid as 0.18 wt.% PEO in water and the matrix liquid as decane ($\rho_1 = 1000$ kg m^{-3}, $\rho_2 = 740$ kg m^{-3}, $\mu_1 = 0.0015$ Ns m^{-2}, $\mu_2 = 0.001$ Ns m^{-2}, $\sigma = 0.032$ N m^{-1} and corresponding non-dimensional parameters are $Oh_1 = 0.0082$, $Oh_2 = 0.0057$, $Bo = 0.136$ and $A = 0.149$). Gradually at $t = 0.52\tau_c$ the drop completely drains into the bulk liquid due to high gravitational pull, leading to complete coalescence. The formation of the satellite drop is observed for the grid resolutions of 150×350, 300×700 and 375×875.

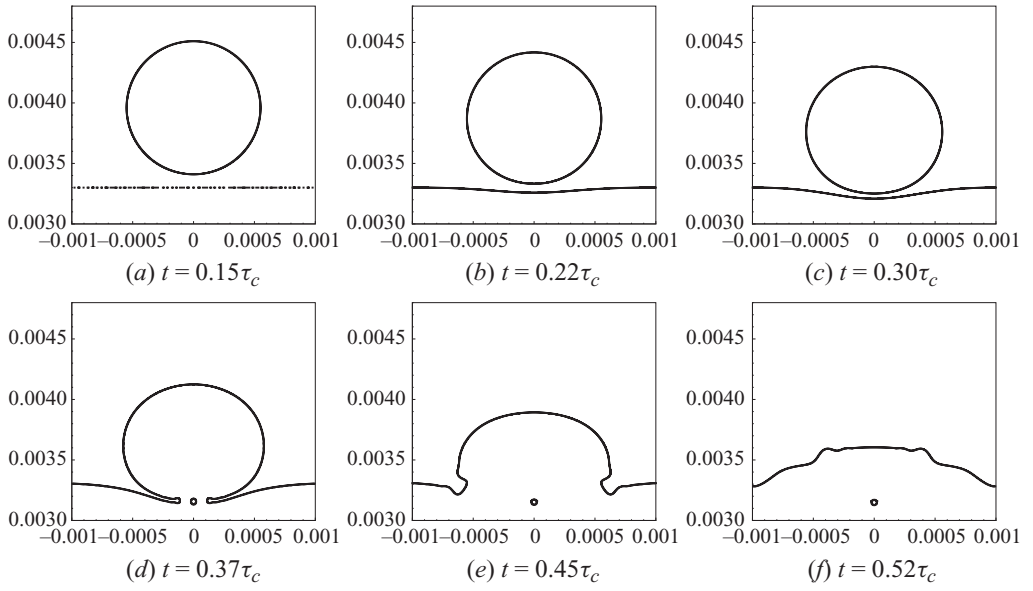

FIGURE 13. Complete coalescence of drop for parameters, $Bo = 9.83$, $Oh_1 = 0.0057$, $Oh_2 = 0.114$ and $A = 0.149$.

The simulations are valid for $Bo = 9.83$. For the smaller Bo, finer grids are required to observe the formation of the satellite drop. Also for very small Bo, when drop comes close to the interface, it does not deform much. So liquid 2 is not trapped between the drop and the interface. This prevents the formation of satellite drop. Admittedly, a full three-dimensional analysis is more appropriate for such a film breakup.

The gravitational pull on the drop may affect the process of partial coalescence as the drop liquid tends to drain out on the underlying bulk liquid. On changing gravity, Bo is changed. All other parameters are kept fixed ($Oh_1 = 0.00533$, $Oh_2 = 0.00387$ and $A = 0.136$) to study the relative effect of gravity with respect to interfacial tension. For low Bond numbers, the process of partial coalescence for different gravity levels does not vary much. In figure 14(a), d_1, d_2 and d_3 represents the primary, secondary and tertiary drop diameters, respectively. It can be seen that the secondary to primary diameter ratio ($\zeta = d_2/d_1$) is independent of Bo and has a fixed value of 0.52, which defines the asymptotic inertio-capillary regime described earlier. As Bo increases beyond 0.09, ζ gradually decreases and at a critical value $Bo_C \approx 7$ total coalescence is observed. After the second pinch-off, the tertiary to secondary drop diameter ratio ($\zeta = d_3/d_2$) is also plotted as shown by dotted lines in the figure.

With increase in Bond number, the pinch-off time (τ_p) gradually decreases, as shown in figure 14(b). As the Ohnesorge numbers are low, the capillary wave in this case can move towards the drop apex with little resistance. Due to increasing downward gravitational pull, more liquid 2 tends to neck the liquid 1 column leading to quick pinch-off. At very high gravitational pull, the liquid 1 column does not form and therefore no pinch-off occurs.

The magnitude of pinch-off time in figure 12(b) and in Blanchette & Bigioni (2009) are different as they are non-dimensionalized by different parameters. Blanchette & Bigioni (2009) have used capillary time $\tau_c = \sqrt{\rho_1 D^3/\sigma}$ and in our simulations $\tau_c = \sqrt{\rho_m D^3/\sigma}$ where ρ_1 is the density of drop liquid and ρ_m is the mean density. Also the Ohnesorge numbers are defined differently in both cases. In the work of

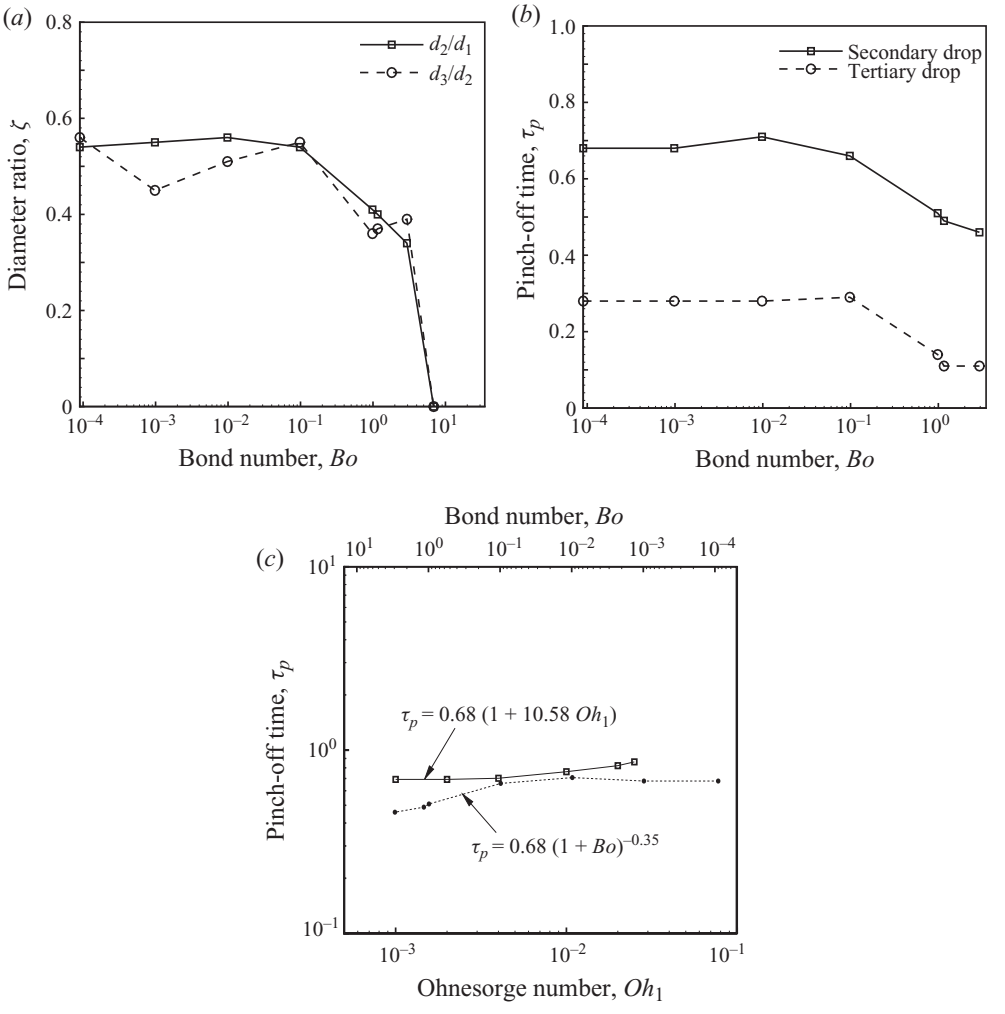

FIGURE 14. (*a*) Diameter ratio (ζ) versus *Bo*. (*b*) Pinch-off time (τ_p) versus *Bo* with other parameters as $Oh_1 = 0.00533$, $Oh_2 = 0.00387$ and $A = 0.136$. (*c*) Pinch-off time (τ_p) as a function of Oh_1 and *Bo*. Length and time are non-dimensional.

Blanchette & Bigioni (2009), $Oh_1 = \mu_1/\sqrt{\rho_1 \sigma D}$ and in this paper two Ohnesorge numbers are used as $Oh_1 = \mu_1/\sqrt{\rho_m \sigma D}$ and $Oh_2 = \mu_2/\sqrt{\rho_m \sigma D}$. Although the time values are significantly different in both the cases, the plots resemble the same qualitative trend. A more appropriate comparison of the results would be with the work of Chen *et al.* (2006*a*). In figure 14(*c*) the pinch-off time (τ_p) is plotted as a function of *Bo* and Oh_1. Chen *et al.* (2006*a*) have obtained the relationship between pinch-off time and Ohnesorge and Bond number as, $\tau_p = 0.77(1 + 9.68Oh)$ and $\tau_p = 0.77(1 + Bo)^{-0.5}$. They have used the liquid 1 density (ρ_1) to calculate the capillary time and the Ohnesorge number. From our simulations, the pinch-off time is related to Ohnesorge number as $\tau_p = 0.68(1 + 10.58Oh_1)$ and to Bond number as $\tau_p = 0.68(1 + Bo)^{-0.35}$.

4.6. *Mechanism of partial coalescence*

The criterion for partial coalescence can be obtained from the critical Ohnesorge numbers (Oh_{1C}, Oh_{2C}) and the Bond number (Bo_C). Figure 15(*a*) show the critical

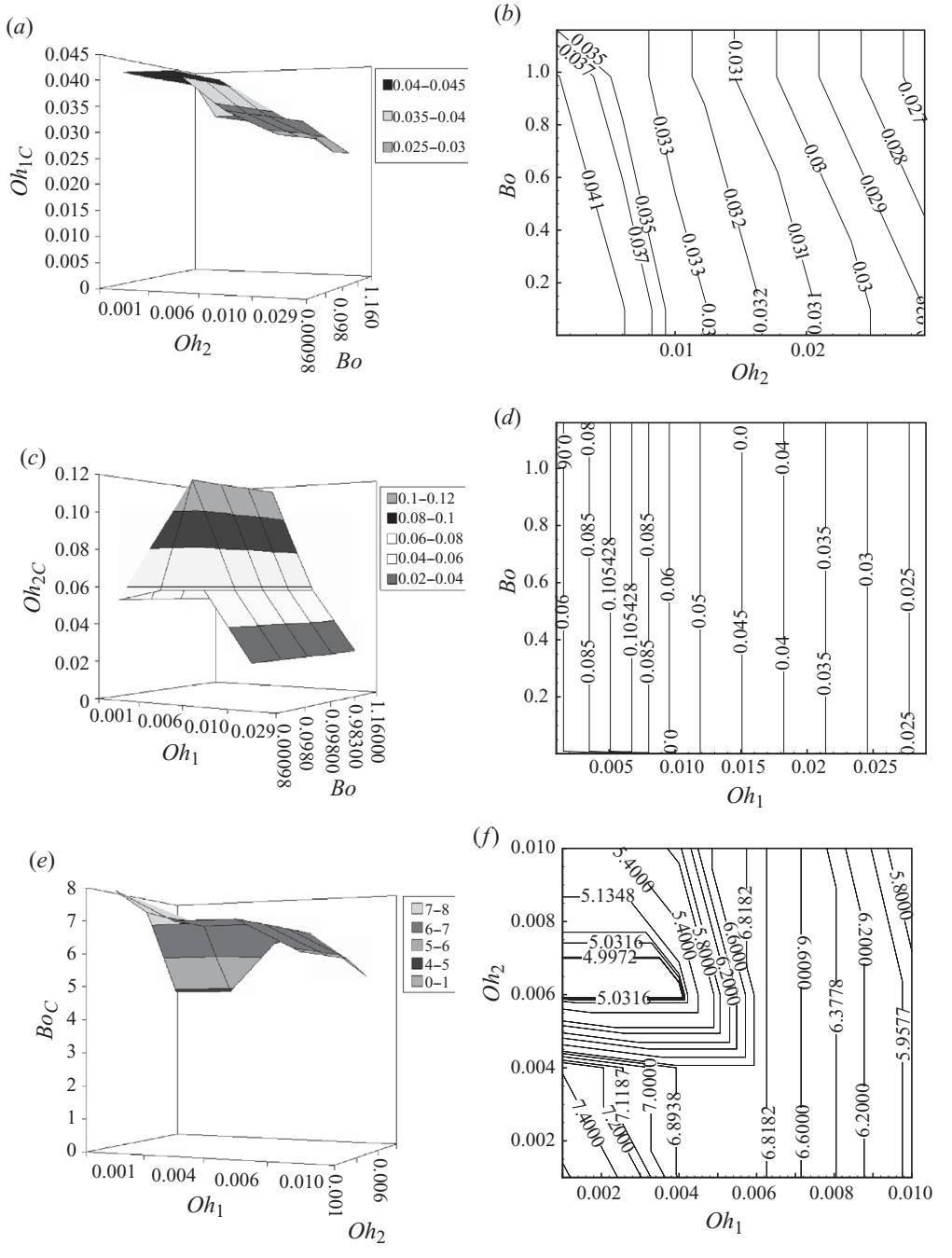

FIGURE 15. (*a*) Surface plot for the critical Ohnesorge number Oh_{1C} as a function of Oh_2 and Bo. (*b*) Contour plot for the critical Ohnesorge number Oh_{1C} as a function of Oh_2 and Bo. (*c*) Surface plot for the critical Ohnesorge number Oh_{2C} as a function of Oh_1 and Bo. (*d*) Contour plot for the critical Ohnesorge number Oh_{2C} as a function of Oh_1 and Bo. (*e*) Surface plot for the critical Bond number Bo_C as a function of Oh_1 and Oh_2. (*f*) Contour plot for the critical Bond number Bo_C as a function of Oh_1 and Oh_2. The Atwood number is $A = 0.136$.

Ohnesorge number for liquid 1 as a function of Oh_2 and Bo. The range of Oh_2 and Bo are $0.001 \leqslant Oh_2 \leqslant 0.029$ and $0.00098 \leqslant Bo \leqslant 1.16$. As Oh_2 increases for given Bo, the critical value gradually decreases. The values of Oh_{1C} remains almost same on increasing Bo.

Figure 15(b) shows the variation of Oh_{2C} with Oh_1 and Bond number. The range of Oh_1 and Bo are $0.001 \leqslant Oh_1 \leqslant 0.029$ and $0.00098 \leqslant Bo \leqslant 1.16$. The trend is different from Oh_{1C}. Here as Oh_1 increases, the critical value (Oh_{2C}) first increases and then decreases. The values of Oh_{2C} does not vary with change in Bo.

Figure 15(c) reveal the variation of Bo_C for different Oh_1 and Oh_2. The range of Oh_1 and Oh_2 are $0.001 \leqslant Oh_1 \leqslant 0.01$ and $0.001 \leqslant Oh_2 \leqslant 0.01$. We see that Bo_C have maximum range for $Oh_1 \leqslant 0.004$ and $Oh_2 \leqslant 0.004$. For $Oh_1 \geqslant 0.006$, Bo_C gradually decreases. For $Oh_2 > 0.004$, Bo_C varies in a complex manner.

From figure 4 the critical value of Ohnesorge numbers for a fixed value of Bond number and the critical value of Bond number for a fixed value of Ohnesorge numbers are obtained. These critical Ohnesorge numbers and Bond number denote a point in each of the phase diagram of figure 15.

Here six different cases are discussed, Case I for partial coalescence when $Oh_1 \approx Oh_2$ and at normal gravity, Case II for partial coalescence when $Oh_1 < Oh_2$ and at normal gravity, Case III for complete coalescence when $Oh_1 \ll Oh_2$ and at normal gravity, Case IV for complete coalescence when $Oh_1 > Oh_2$ and at normal gravity, Case V for partial coalescence when $Oh_1 \approx Oh_2$ and at gravity higher than normal gravity and Case VI for complete coalescence when $Oh_1 \approx Oh_2$ and at gravity much higher than normal gravity. The streamlines, u-velocity and v-velocity contours are plotted for each case. The darker shade indicates the maximum negative value whereas the lighter-shade represents maximum positive values of the velocity components.

Figure 16(a) shows the streamlines, u-velocity and v-velocity contours of Case I, respectively. The other parameters are $Bo = 0.0958$, $Oh_1 = 0.0058$ and $Oh_2 = 0.0041$. When the drop touches the interface, the thin film beneath ruptures and then capillary waves set in. The capillary waves are generated by the opening of the neck at the early stage of coalescence. Some of these waves move up towards the drop apex and the rest move away from the drop towards the side. The streamline shows the movement of the capillary wave towards the apex of the drop. The instantaneous location during the evolution is identified as A. For the capillary waves, with a wavelength much smaller than the drop radius, the wave velocity is given by $\sqrt{(\sigma k/\rho_m)}$, where k is the wavenumber. Such waves carry momentum to distort the drop when they converge on the summit (Blanchette & Bigioni 2006). As more capillary waves converge at the apex, the vertical collapse of the drop is retarded. Thus horizontal collapse leads to the pinch-off of the drop. This competition between the horizontal and vertical momentum is seen in u-velocity and v-velocity contours.

A different case of partial coalescence, Case II, is shown in figure 16(b). The $Bo = 0.0958$, $Oh_1 = 0.0058$ and $Oh_2 = 0.0589 (Oh_1 < Oh_2)$. Here the viscosity of dispersed liquid (liquid 2) is very high compared with liquid 1. Unlike the previous case, the drop does not convert to an elongated column shape. The velocity vector plot shows that the drop is always below the dotted line. The dotted line signifies the initial height of the drop.

In the case of complete coalescence, Cases III and IV, the vertical collapse exceeds the horizontal collapse, as shown in figures 17(a) and 17(b). The non-dimensional parameters are $Bo = 0.0958$, $Oh_1 = 0.0058$ and $Oh_2 = 0.1179 (Oh_1 \ll Oh_2)$ for Case III and $Oh_1 = 0.0412$ and $Oh_2 = 0.0058 (Oh_1 > Oh_2)$ for Case V. Even though the capillary waves move towards the drop apex, the vertical elongation of the drop

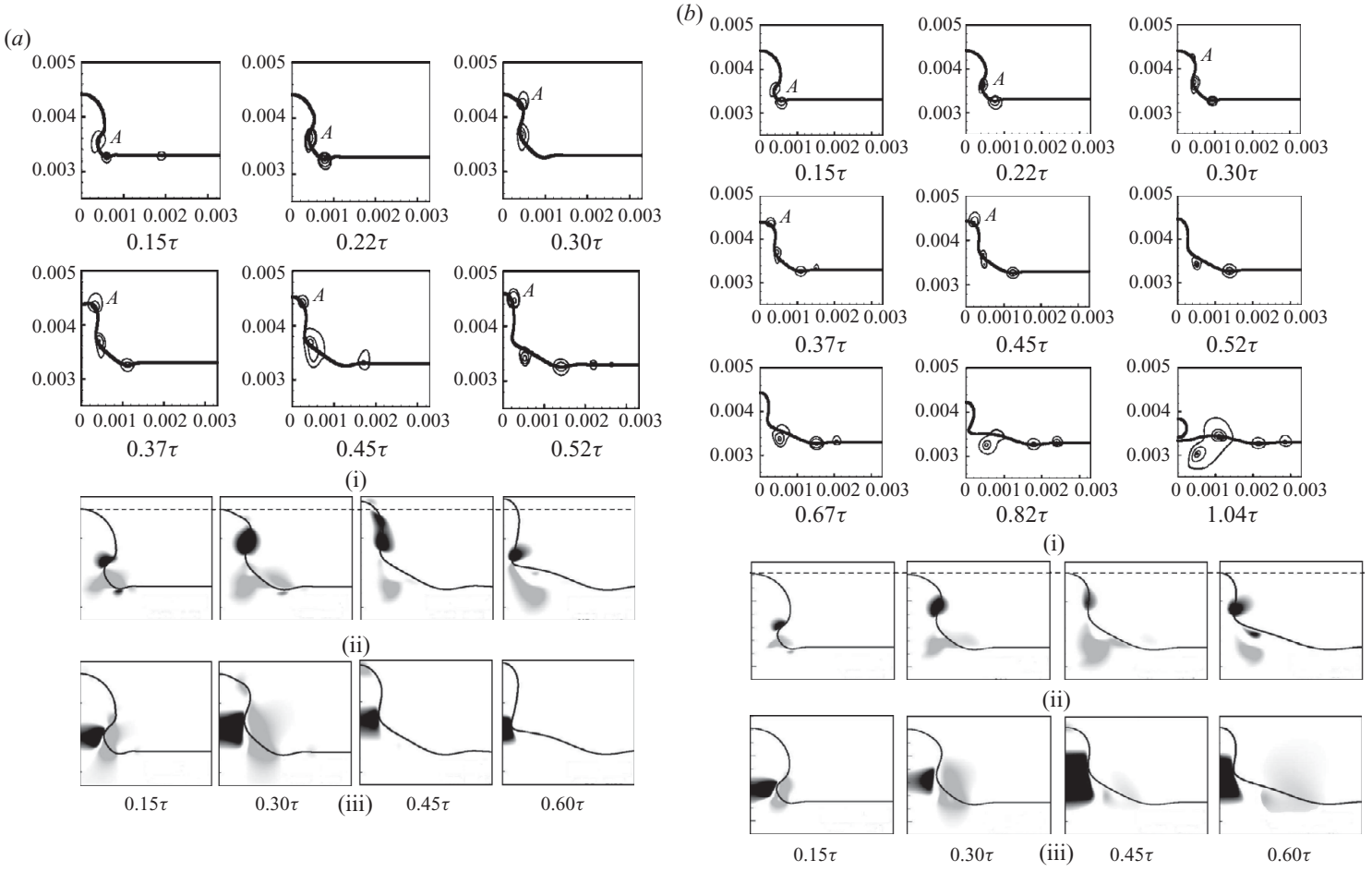

FIGURE 16. Streamline plot, u-velocity contour and v-velocity contour for (*a*) partial coalescence for nearly equal Oh_1 and Oh_2 (Case I): $Oh_1 = 0.0058$ and $Oh_2 = 0.0041$. (*b*) Partial coalescence for intermediate value of Oh_2 (Case II): $Oh_1 = 0.0058$ and $Oh_2 = 0.0589$. The other parameters are $Bo = 0.0958$ and $A = 0.136$. In third row the horizontal velocity is shown with light and dark shade indicating motion from and towards the centre, respectively. In bottom row the vertical velocity is shown with light and dark shade indicating upward and downward motion, respectively.

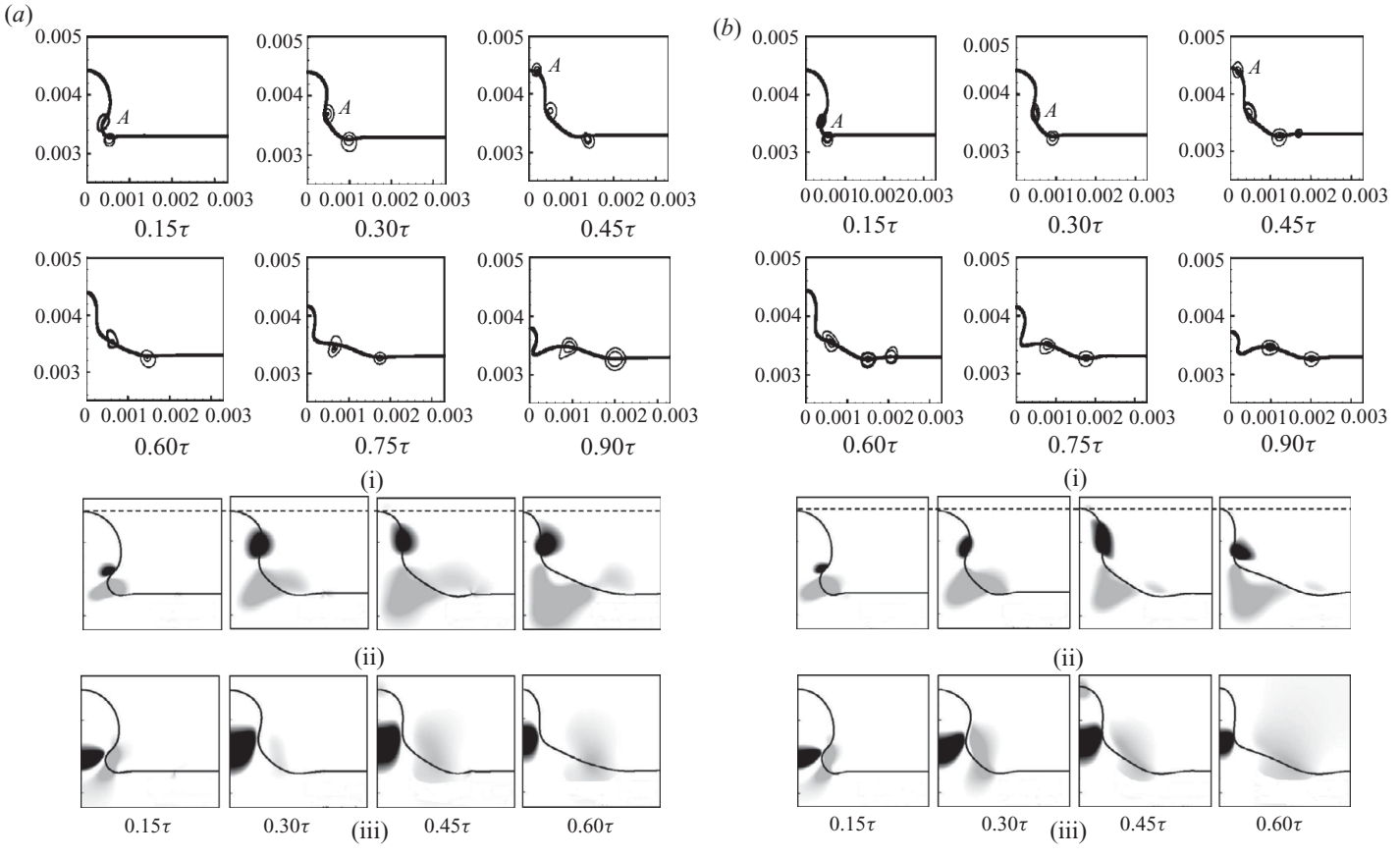

FIGURE 17. Streamline plot, u-velocity contour and v-velocity contour for (*a*) complete coalescence for high value of Oh_2 (Case III): $Oh_1 = 0.0058$ and $Oh_2 = 0.1179$. (*b*) Complete coalescence for intermediate value of Oh_1 (Case IV): $Oh_1 = 0.0412$ and $Oh_2 = 0.0058$. The other parameters are $Bo = 0.0958$ and $A = 0.136$. In third row the horizontal velocity is shown with light and dark shade indicating motion from and towards the centre, respectively. In bottom row the vertical velocity is shown with light and dark shade indicating upward and downward motion, respectively.

is restricted by high viscosity. The drop height (height of the elongated column) is smaller than in the earlier case (figure 16*a*). The coalescence is complete or total despite the presence of capillary waves.

Similar phenomena to those in figure 16(*a*) occur for high Bond numbers (Case V). In figure 18(*a*) shows the case with $Bo = 1.966$, $Oh_1 = 0.0058$ and $Oh_2 = 0.0041$. Due to more gravitational pull, the drop sinks in and the interface becomes curved before a hole is created. After the hole has been formed, the capillary wave moves in a similar manner to that shown in figure 16(*a*). The only difference is that due to more draining of the liquid 1, the secondary drop formed is smaller in this case.

After increasing the Bond number beyond a certain limit (Case VI), it is seen that the secondary drop does not pinch off any more. Such phenomena are shown in figure 18(*b*). The pertinent input parameters are $Bo = 6.88$, $Oh_1 = 0.0058$ and $Oh_2 = 0.0041$. Here the downward horizontal motion of the drop is very high, as shown by the darker-shade in v-velocity contours. More gravity leads to more vertical momentum and thus pinch-off cannot occur. The capillary wave formed could not move towards the drop apex due to the high downward pull.

For different Atwood, Bond and Ohnesorge numbers, the maximum drop height, h_{drop}, and the maximum crater depth, h_{crater} after pinch-off are plotted. The measurements are made from the initial liquid–liquid interface. From figure 19, it is clear that the Atwood number has a negligible effect on h_{drop} and h_{crater}. As Bo increases, the drop height and crater depth continue to have constant values until at very high Bo the maximum depth of the crater increases and maximum height of the drop gradually decreases. This is due to a greater downward gravitational pull. A similar trend is observed for increasing Ohnesorge number but the rate of change is less in this case. As viscosity of the drop increases, the size of the secondary drop formed decreases. After pinch-off the interface crater moves to a greater depth. It is interesting to note that in all the cases, the average value of $h_{drop} \approx 1.2$ and $h_{crater} \approx 0.045$.

4.7. *Transition from partial to complete coalescence*

To understand the mechanism more clearly, the neck radius (R_{neck}) for the above six cases is plotted with respect to time in figure 20(*a*). For the case of partial coalescence (Case I and Case II) the neck radius oscillates only once and then reduces to zero. In the case of complete coalescence due to high viscosity (Case III and Case IV), the neck radius oscillate twice with time whereas in the case of complete coalescence due to high gravity (Case V and Case VI) the neck radius reduce in one oscillation.

The transition from partial to complete coalescence due to increasing viscosity of liquid 2 with other parameters as $Bo = 0.0958$, $Oh_1 = 0.0058$ and $A = 0.136$ is shown in figure 20(*b*). Two cases of partial coalescence corresponding to Cases I and II are illustrated, which shows that at intermediate viscosity of liquid 2 ($Oh_2 = 0.0589$), the pinch-off of the secondary drop takes more time. The transition to complete coalescence is found at $Oh_2 = 0.1179$ corresponding to Case III, where the drop oscillates twice before collapsing into the bulk liquid. As the viscosity is increased more to $Oh_2 = 0.3$ corresponding to figure 11, the number of oscillations reduces. For very high $Oh_2 = 0.589$, the contact of the drop with the interface takes more time and so the curve in figure 20(*b*) is seen to shift towards the right, but the number of oscillations does not change. For high viscosity, it is seen that the maximum neck radius increases, which indicates more spreading of the drop before collapsing. Similarly, when the liquid 1 Ohnesorge number is increased to $Oh_1 = 0.3$ corresponding to figure 10, the neck oscillates only once during complete coalescence.

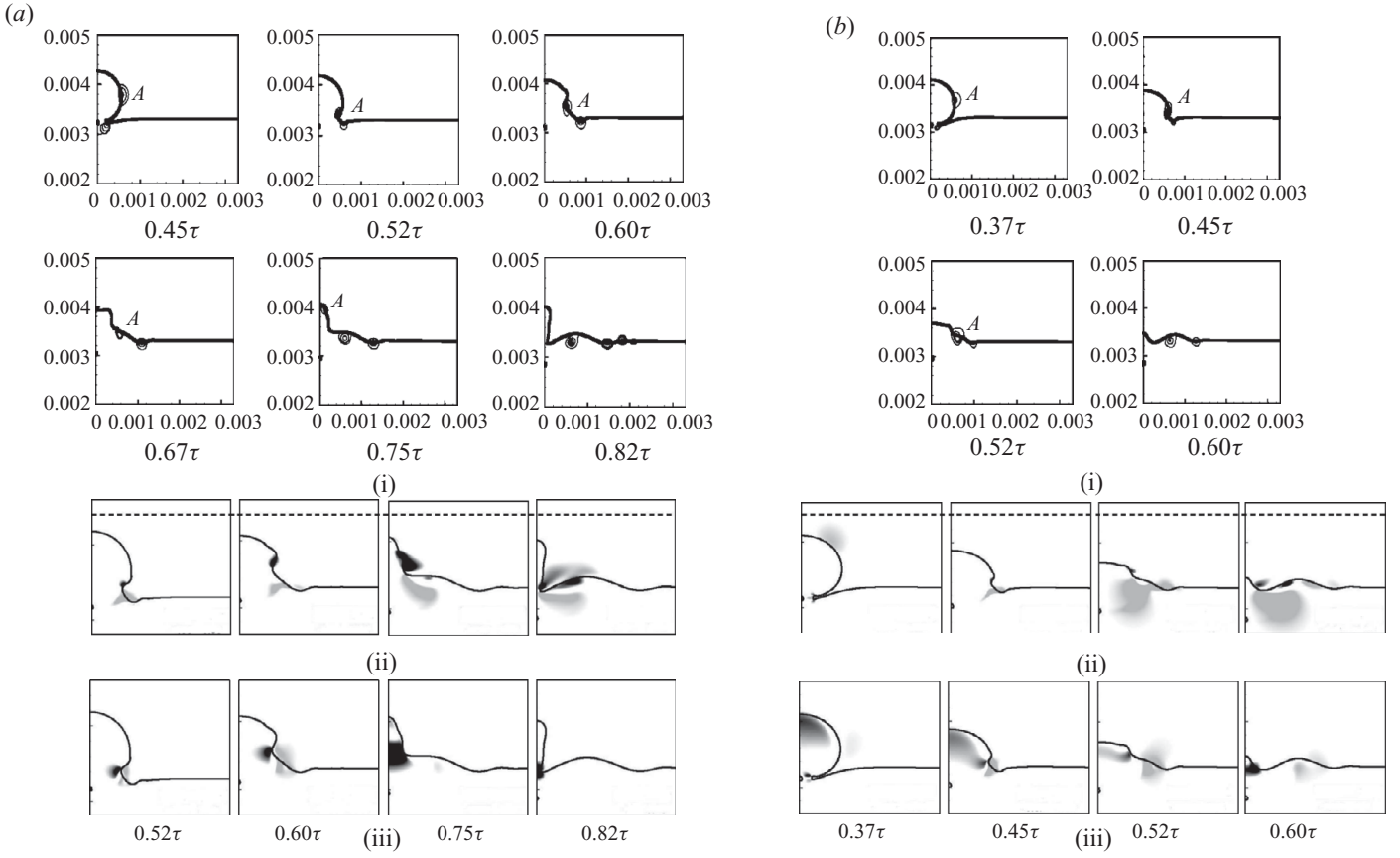

FIGURE 18. Streamline plot, u-velocity contour and v-velocity contour for (a) partial coalescence for for nearly equal Oh_1 and Oh_2 and intermediate gravity (Case V): $Bo = 1.966$. (b) Complete coalescence for for nearly equal Oh_1 and Oh_2 and intermediate gravity (Case VI): $Bo = 6.88$. The other parameters are $Oh_1 = 0.0058$, $Oh_2 = 0.0041$ and $A = 0.136$. In third row the horizontal velocity is shown with light and dark shade indicating motion from and towards the centre, respectively. In bottom row the vertical velocity is shown with light and dark shade indicating upward and downward motion, respectively.

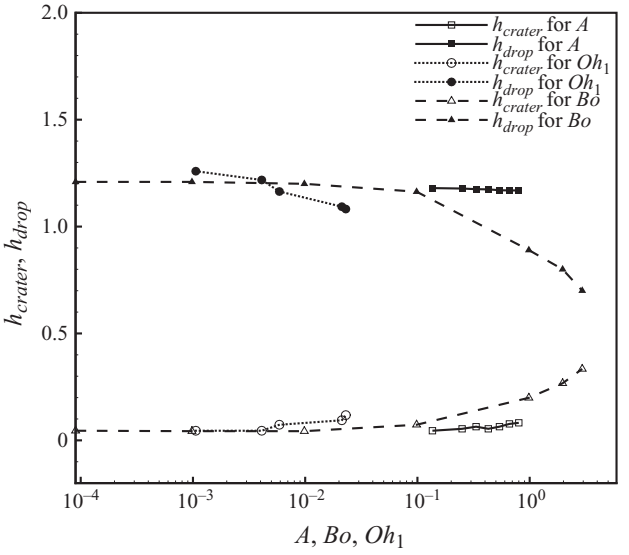

FIGURE 19. Maximum drop height (h_{drop}) and maximum crater depth (h_{crater}) versus Atwood, Bond and Ohnesorge numbers. Length is non-dimensional.

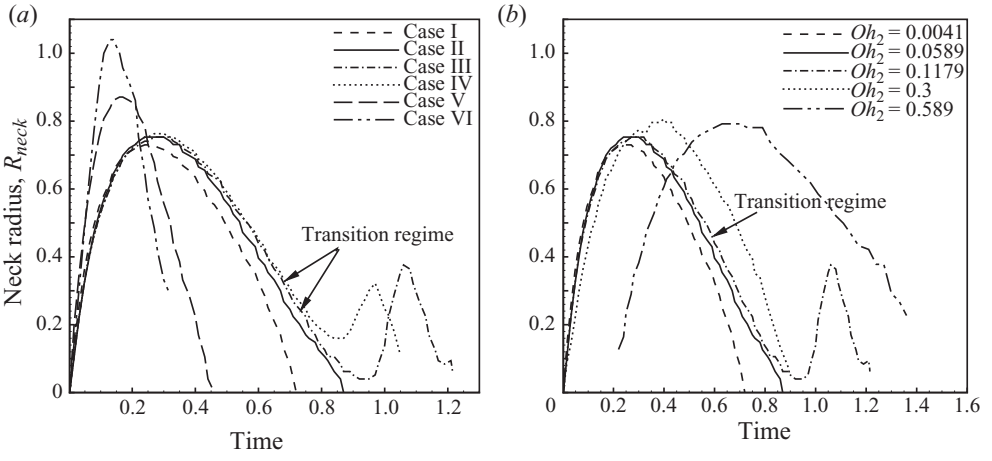

FIGURE 20. Radius of neck (R_{neck}) versus time for Case I to Case VI. (b) Radius of neck (R_{neck}) versus time for different values of Oh_2 showing transition from partial to complete coalescence with other parameters as $Bo = 0.0958$, $Oh_1 = 0.0058$ and $A = 0.136$. Length and time are non dimensional.

Thus it is clear from the above results that number of oscillations of the neck radius is a critical parameter which decides the transition from partial to complete coalescence.

In this transition regime where the neck radius oscillates twice, we get self-silimar column profiles. In the complete coalescence process in figure 9, it is seen that the profiles from $t = 0.39\tau_c$ to $0.6\tau_c$ are similar and again the profiles from $t = 1.08\tau_c$ to $1.16\tau_c$ are similar. These profiles are shown in figures 21(a) and 21(c). As time elapses, the column grows in height and later as the gravity effect dominates, the column stops growing. They both show a self-similar character for the column structure, which is shown in figures 21(b) and 21(d). By characterizing the column's growth profiles using

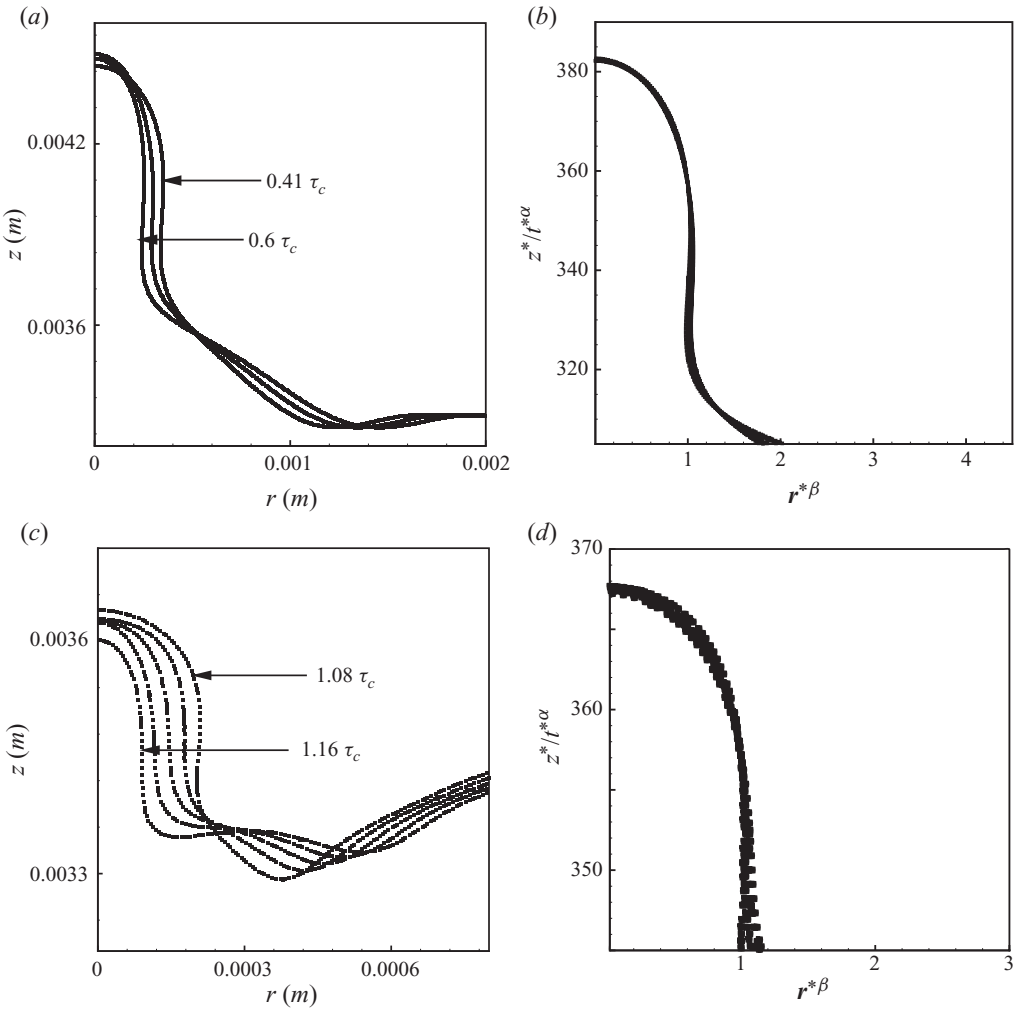

FIGURE 21. Self-similar structure of the column profile: the interface profiles are shown on the left. The right-hand side shows the same curves rescaled (*a*), (*b*) for $t = 0.39\tau_c$ to $0.6\tau_c$ and (*c*), (*d*) for $t = 1.08\tau_c$ to $1.16\tau_c$.

power-law scaling, one could derive useful information about the dynamics of drop coalescence. We have examined the sidewall profile of the column and excluded the base of the column. All the profiles starting from $t = 0.39\tau_c$ until $0.6\tau_c$ collapse on a single profile shown on figure 21(*b*). For $t = 1.08\tau_c$ to $1.16\tau_c$ again the profiles collapse on a single profile (figure 21*d*).

The column profile is fitted with the general solution form for the kinetic free-surface problem by Hogrefe *et al.* (1998): $z = at^{\lambda}(rt^{\eta})^{\nu}$. Here z and r are the coordinates of a point located on the column sidewall. The original dimensional frame (z, r, t) is non-dimensionalized to (z^*, r^*, t^*) by scaling z and r with drop radius, t is scaled using viscous time, $\tau_v = D^2\rho_m/\mu_m$. Our fitting function is of the form, $z^*/t^{*\alpha} = ar^{*\beta}$. The value of α and β comes out to be -2 and 1, respectively, and the value of $a = 0.0014$ for $t = 0.39\tau_c$ to $0.6\tau_c$ and $\alpha = -2$, $\beta = 1$ and $a = 0.01$ for $t = 1.08\tau_c$ to $1.16\tau_c$. The rescaling gives the collapsed profiles as exhibited in figures 21(*b*) and

21(*d*). In particular, we observe that the column height evolves as t^{-2}. The height of the surface is linear with respect to the radius indicating a cylindrical shape of the profile. Such self-similarity is also observed for complete coalescence when Oh_2 is slightly larger than Oh_1. Duchemin, Josserand & Clavin (2005) showed the asymptotic behaviour of the spikes due to Rayleigh–Taylor instability evolving as t^2. Duchemin *et al.* (2002) have shown this similarity when a bubble burst at a free surface. They derived a self-similar flow occurring when the conical cavity and the cusp form followed by jet formation. Deng, Anilkumar & Wang (2007) also fitted the high-speed thin jet following bubble pinch-off to a power-law model. The scaling behaviour for self-similar dynamics in case of capillary-inertia regime gives the value of $\alpha = 0.667$. In case of thin high speed jet or cavity collapse inside a liquid body, the value of α varies between 0.4 and 0.667. In these cases as the α is positive and less then one, smaller value of α indicates higher singularity of the jet.

5. Discussion

Charles & Mason (1960*a*) have suggested that the partial coalescence was due to a Rayleigh–Plateau instability. Blanchette & Bigioni (2006) have argued that it is the convergence of the capillary waves on the drop apex which leads to secondary drop pinch off. Recently Gilet *et al.* (2007*a*) have shown that the convergence of the capillary waves cannot be the only mechanism responsible for partial coalescence. They showed that when Oh_1 is high, a mechanism is responsible for enhancing the emptying of the droplet, resulting in a premature total coalescence. Inversely, when Oh_2 is high, another mechanism has to aid the horizontal collapse. However, when Oh_2 is too large, it has an opposite effect of weakening of the horizontal collapse. From the six cases that have been mentioned in §4.6 it is seen that the important criterion for partial coalescence is the increasing horizontal momentum of the drop relative to the vertical momentum. This can be accomplished either by changing the viscosity or by changing the gravity within limits. Figure 22 depicts the dominant movement in the above six cases. The dotted line indicates the initial liquid–liquid interface. In the Case I ($Oh_1 \approx Oh_2$), the liquid column is stretched upwards to a long height and liquid 2 forces inwards to do the pinch-off. In the Case II ($Oh_1 < Oh_2$), the height of the liquid column is lower due to the higher viscosity of liquid 2, but the higher viscosity increases the horizontal collapse. So the drop pinches off before collapsing. During the Case III ($Oh_1 \ll Oh_2$), at very high viscosity of liquid 2, the pinch-off is prevented and viscous liquid 2 pushes the entire drop to coalesce completely. In the Case IV ($Oh_1 > Oh_2$), due to the high viscosity of liquid 1, the capillary waves get damped out and the drop coalesces totally. It can be concluded that for a low Oh_1 value ($= 0.0058$), when $(Oh_1/Oh_2) \approx 1$, the pinch-off of secondary drop occurs. As this ratio decreases to 0.1, the partial coalescence phenomenon still occurs but as the ratio is further decreased to 0.01, there is no more pinch-off. In contrast, for a low Oh_2 value ($= 0.0058$), as Oh_1 is increased by a small amount, $Oh_1 = 0.0412 (Oh_1/Oh_2 \approx 10)$, the drop completely coalesces. In the case of a high viscosity of liquid 1, more mass of liquid 2 is displaced. Hence as Oh_1 is increased, an additional movement is induced which tends to accelerate the emptying of the droplet. More viscous diffusion leads to vertical collapse of the liquid column. In liquid 2, such an induced movement enhances the horizontal collapse. When Oh_2 is intermediate, the horizontal collapse is confined to regions lower than the equator of the initial droplet, and this leads to partial coalescence. In contrast, when Oh_2 is high, the viscous diffusion entrains liquid 1 at higher latitudes and the vertical extension

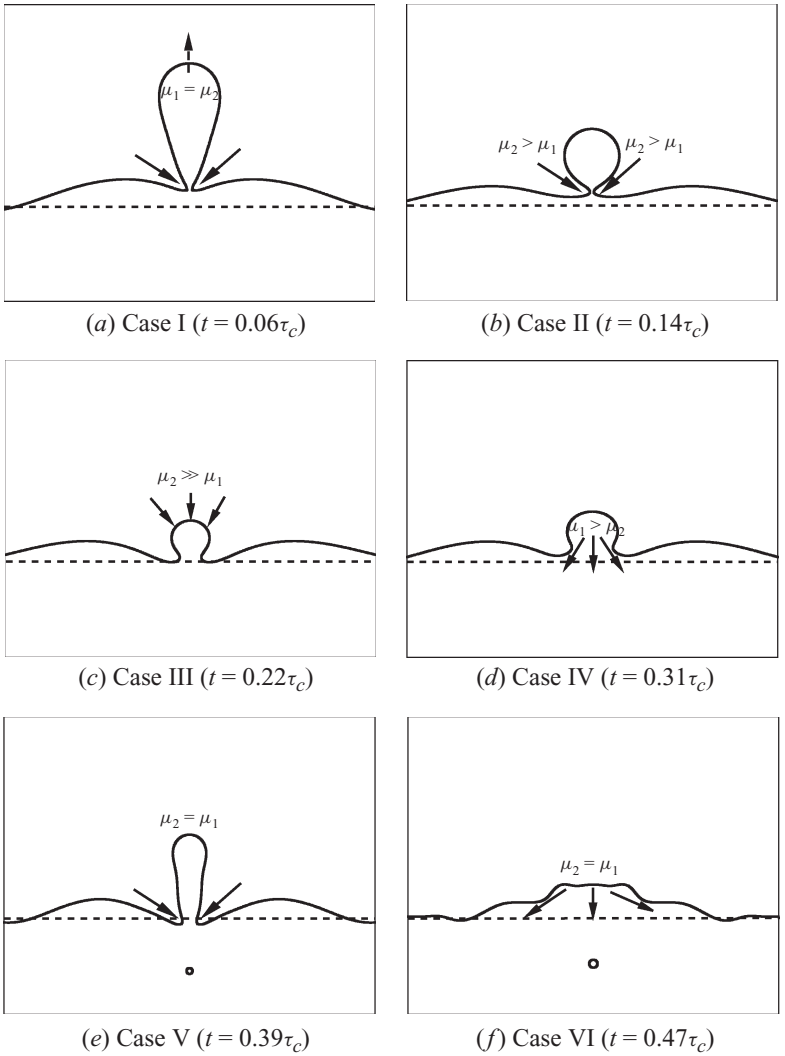

(*a*) Case I ($t = 0.06\tau_c$) (*b*) Case II ($t = 0.14\tau_c$)

(*c*) Case III ($t = 0.22\tau_c$) (*d*) Case IV ($t = 0.31\tau_c$)

(*e*) Case V ($t = 0.39\tau_c$) (*f*) Case VI ($t = 0.47\tau_c$)

FIGURE 22. Dominant movements of liquid for Case I to Case VI.

of the horizontal collapse is greater, so the coalescence becomes total. The Case V ($Oh_1 \approx Oh_2$, intermediate Bo) illustrates the following. The pinch-off is similar to that in the Case I, but as can be seen from the figure, the necking is below the initial liquid–liquid interface due to more downward pull. Case VI ($Oh_1 \approx Oh_2$, high Bo) shows the total collapse of the drop due to the large downward vertical movement of the drop for high gravitational pull. Thus it is seen that whether the drop will completely coalesce or it will pinch off secondary droplet depends on the dominant direction of flows acting on the drop.

6. Conclusions

This paper has mainly focused on the various outcomes of the partial coalescence process. The critical behaviour of the liquids during the formation of daughter

drops, both secondary drops, tertiary drops and the satellite drops has been revealed. The most important results that are discussed in this study can be summarized as follows:

When liquid drop impacts on a liquid–liquid interface, for very small drops (corresponding $Oh_1 > 0.035$, $Oh_2 = 0.0058$, $Bo = 0.0958$ and $A = 0.136$) and very large drops (corresponding $Bo > 7$, $Oh_1 = 0.00533$, $Oh_2 = 0.00387$ and $A = 0.136$), the phenomena of partial coalescence do not occur. Within this range, the process can be divided into three regimes, depending on the different forces, namely viscous force, surface tension force, inertia force and buoyancy force. Coalescence cascade is observed in the inertio-capillary regime, which is self-similar in nature. The daughter drop shape changes from prolate to oblate and then to spherical before it comes in contact with the interface. Sometimes for large drops, two secondary drops are formed. The first pinch-off is due to partial coalescence and the second is due to Rayleigh-Plateau instability. Within the inertio-capillary regime, the partial coalescence phenomena is independent of Atwood number.

We propose the mechanism by which transition from complete coalescence to partial coalescence occurs. Gilet *et al.* (2007*a*) have explained the huge difference between critical Ohnesorge numbers in both fluids by suspecting the presence of viscous forces which effect partial coalescence. In the present work we have numerically established that it is the competition between the horizontal and vertical momentum of the drop which determines the transition between the two regimes of coalescence. The capillary wave converge at the drop apex. Furthermore, when the horizontal momentum exceeds the vertical momentum, a daughter drop pinches out. Different forces for different flow parameters determine the outcome. The critical Ohnesorge numbers (Oh_{1C}, Oh_{2C}) and the Bond number (Bo_C) show how different parameters effect the partial coalescence process. The maximum height attained by the drop (h_{drop}) and the maximum depth of the crater (h_{crater}) does not vary much for a wide range of Bond number and Ohnesorge numbers.

A transition regime between partial and complete coalescence with increasing Ohnesorge number is defined. In this regime the neck oscillates twice before collapsing into the liquid. For further increase in Ohnesorge number the oscillation again reduces to one. Within this transition regime the column profiles in a certain time range show power law scaling. Duchemin *et al.* (2002) have shown such self-similarity of the profiles before jet formation when an air bubble bursts at the free surface.

In the experimental work of Mohamed-Kassim & Longmire (2003, 2004), the thin film below the drop ruptured asymmetrically. To capture this kind of rupture numerically, three-dimensional studies are needed. Even the initial shape of the drop is taken to be spherical and it approaches the interface at specified velocity. This kind of initial conditions are seen in the numerical work of Morton *et al.* (2000). In order to see the effect of drop shape more parametric study is needed. Further study is to be done on the controlling parameters for partial coalescence. Some recent studies by Gilet, Vandewalle & Dorbolo (2007*b*) have shown that the partial coalescence can be prevented by using vertically vibrating bath. Other studies include the use of surfactant to prevent the pinch-off. Also the process of partial coalescence when two drops of unequal size comes in contact (Zhang *et al.* 2009) is to be investigated numerically.

The authors are thankful to Professor Stephane Zaleski of UPMC, Paris for many insightful discussions.

REFERENCES

Agarwal, D. K., Welch, S. W. J., Biswas, G. & Durst, F. 2004 Planar simulation of bubble growth in film boiling in near-critical water using a variant of the VOF method. *J. Heat Transfer* **126**, 329–338.

Aryafar, H. & Kavehpour, H. P. 2006 Drop coalescence through planar surfaces. *Phys. Fluids* **18**, 072105(1)–072105(6).

Berry, E .X. & Reinhardt, R. L. 1974 Analysis of cloud drop growth by collection. III. Accretion and self-collection. *J. Atmos. Sci.* **31**, 2118–2126.

Bhakta, A. & Ruckenstein, E. 1997 Decay of standing foams: drainage, coalescence and collapse. *Adv. Colloid Interface Sci.* **70**, 1–124.

Blanchette, F. & Bigioni, T. P. 2006 Partial coalescence of drops at liquid interfaces. *Nat. Phys.* **2**, 254–257.

Blanchette, F. & Bigioni, T. P. 2009 Dynamics of drop coalescence at fluid interfaces. *J. Fluid Mech.* **620**, 333–352.

Brackbill, J. U., Kothe, D. B. & Zemach, C. 1992 A continuum method for modelling surface tension. *J. Comput. Phys.* **100**, 335–354.

Cai, Y. K. 1989 Phenomena of a liquid drop falling to a liquid surface. *Exp. Fluids.* **7**, 388–394.

Chakraborty, I., Ray, B., Biswas, G., Durst, F., Sharma, A. & Ghoshdastidar, P. S. 2009 Computational investigation on bubble detachment from submerged orifice in quiescent liquid under normal and reduced gravity. *Phys. Fluids* **21**, 062103(1)–062103(17).

Chang, Y. C., Hou, T. Y., Merriman, B. & Osher, S. 1996 A level-set formulation of eulerian interface capturing methods for incompressible fluid flows. *J. Comput. Phys.* **124**, 449–464.

Charles, G. E. & Mason, S. G. 1960*a* The coalescence of liquid drops with flat liquid/liquid interfaces. *J. Colloid Sci.* **15**, 236–267.

Charles, G. E. & Mason, S. G. 1960*b* The mechanism of partial coalescence of liquid drops at liquid/liquid interfaces. *J. Colloid Sci.* **15**, 105–122.

Chen, X., Mandre, S. & Feng, J. J. 2006*a* Partial coalescence between a drop and a liquid–liquid interface. *Phys. Fluids* **18**, 051705(1)–051705(4).

Chen, X., Mandre, S. & Feng, J. J. 2006*b* An experimental study of the coalescence between a drop and an interface in newtonian and polymeric liquids. *Phys. Fluids* **18**, 092103(1)–092103(14).

Ching, B., Golay, M. W. & Johnson, T. J. 1984 Droplet impacts upon liquid surfaces. *Science* **226**, 535–537.

Deng, Q., Anilkumar, A. V. & Wang, T. G. 2007 The role of viscosity and surface tension in bubble entrapment during drop impact onto a deep liquid pool. *J. Fluid Mech.* **578**, 119–138.

Duchemin, L., Josserand, C. & Clavin, P. 2005 Asymptotic behaviour of the Rayleigh–Taylor instability. *Phys. Rev.* L **94**, 224501(1)–224501(4).

Duchemin, L., Popinet, S., Josserand, C. & Zaleski, S. 2002 Jet formation in bubbles bursting at free surface. *Phys. Fluids* **14**, 3000–3008.

Fedorchenko, A. I. & Wang, A. B. 2004 On some common features of drop impact on liquid surfaces. *Phys. Fluids.* **16**, 1349–1365.

Gerlach, D., Tomar, G., Biwas, G. & Durst, F. 2006 Comparison of volume-of-fluid methods for surface tension-dominant two-phase flows. *Intl J. Heat Mass Transfer* **49**, 740–754.

Gilet, T., Mulleners, K., Lecomte, J. P., Vandewalle, N. & Dorbolo, S. 2007*a* Critical parameters for the partial coalescence of a droplet. *Phys. Rev.* E **75**, 036303(1)–036303(14).

Gilet, T., Vandewalle, N. & Dorbolo, S. 2007*b* Controlling the partial coalescence of a droplet on a vertically vibrated bath. *Phys. Rev.* E **76**, 035302(1)–035302(4).

Harlow, F. H. & Welch, J. E. 1965 Numerical calculation of time-dependent viscous incompressible flow of fluid with free surface. *Phys. Fluids* **8**, 2182–2189.

Hirt, C. W. & Nichols, B. D. 1981 Volume of fluid (VOF) method for the dynamics of free boundaries. *J. Comput. Phys.* **39**, 201–225.

Hogrefe, J. E., Peffley, N. L., Goodridge, C. L., Shi, W. T., Hentschel, H. G. E. & Lathrop, D. P. 1998 Power-law singularities in gravity-capillary waves. *Physica* D **123**, 183–205.

Honey, E. M. & Kavehpour, H. P. 2006 Astonishing life of a coalescing drop on a free surface. *Phys. Rev.* E **167**, 027301(1)–027301(4).

Jayaratne, O. W. & Mason, B. J. 1964 The coalescence and bouncing of water drops at an air/water interface. *Proc. R. Soc. Lond.* **280**, 545–565.

Liow, J. L. 2001 Splash formation by spherical drops. *J. Fluid Mech.* **427**, 73–105.

Marucci, G. 1969 A theory of coalescence. *Chem. Engng Sci.* **24**, 975–985.

Menchaca-Rocha, A., Martinez-Davalos, A., Nunez, R., Popinet, S. & Zaleski, S. 2001 Coalescence of liquid drops by surface tension. *Phys. Rev.* E **63**, 046309(1)–046309(5).

Mohamed-Kassim, Z. & Longmire, E. K. 2003 Drop impact on a liquid/liquid interface. *Phys. Fluids* **15**, 3263–3273.

Mohamed-Kassim, Z. & Longmire, E. K. 2004 Drop coalescence through a liquid/liquid interface. *Phys. Fluids* **16**, 2170–2181.

Morton, D., Rudman, M. & Liow, J. L. 2000 An investigation of the flow regimes resulting from splashing drops. *Phys. Fluids* **12**, 747–763.

Osher, S. & Sethian, J. A. 1988 Fronts propagating with curvature-dependent speed: Algorithm based on Hamilton–Jacobi formulations. *J. Comput. Phys.* **79**, 12–49.

Pikhitsa, P. & Tsargorodskaya, A. 2000 Possible mechanism for the multistage coalescence of a floating droplet on the air/liquid interface. *Colloids Surf.* A **167**, 287–291.

Popinet, S. & Zaleski, S. 1999 A front tracking algorithm for the accurate representation of surface tension. *Intl J. Numer. Methods Fluids* **30**, 775–793.

Puckett, E. G., Almgren, A. S., Bell, J. B., Marcus, D. L. & Rider, W. J. 1997 High-order projection method for tracking fluid interface in variable density incompressible flows boundaries. *J. Comput. Phys.* **130**, 269–282.

Raes, F., Dingenena, R. V., Vignatia, E., Wilsona, J., Putauda, J. P., Seinfeldb, J. H. & Adams, P. 2000 Formation and cycling of aerosols in the global troposphere. *Atmos. Environ.* **34**, 4215–4240.

Rein, M. 1996 The transitional regime between coalescing and splashing drops. *J. Fluid Mech.* **306**, 145–165.

Rudman, M. 1997 Volume-tracking methods for interfacial flow calculations. *Intl J. Numer. Methods Fluids* **24**, 671–691.

Sarpkaya, T. 1996 Vorticity, free surface, and surfactants. *Annu. Rev. Fluid Mech.* **28**, 83–128.

Schotland, R. M. 1960 Experimental results relating to the coalescence of water drops with water surfaces. *Discuss. Faraday Soc.* **30**, 72–77.

Sethian, J. A. 1999 *Level Set Methods and Fast Marching Methods*. Cambridge University Press.

Sussman, M. & Puckett, E. G. 2000 A coupled level-set and volume-of-fluid method for computing 3D and axisymmetric incompressible two-phase flows. *J. Comput. Phys.* **162**, 301–337.

Thompson, J. J. & Newall, H. F. 1885 On the formation of vortex rings by drops falling into liquids and some allied phenomena. *Proc. R. Soc. Lond.* **39**, 417–436.

Thoroddsen, S. T., Etoh, T. G. & Takehara, K. 2003 Air entrapment under an impacting drop. *J. Fluid Mech.* **478**, 125–134.

Thoroddsen, S. T. & Takehara, K. 2000 The coalescence cascade of a drop. *Phys. Fluids* **12**, 1265–1267.

Thoroddsen, S. T., Takehara, K. & Etoh, T. G. 2005 The coalescence speed of a pendent and a sessile drop. *J. Fluid Mech.* **527**, 85–114.

Tomar, G., Biswas, G., Sharma, A. & Agarwal, A. 2005 Numerical simulation of bubble growth in film boiling using CLSVOF method. *Phys. Fluids* **17(1)**, 112103(1)–112103(13).

VanderVorst, H. A. 1992 Bi-cgstab: a fast and smoothly converging variant of Bi-CG for solution of non-symmetric linear systems. *SIAM J. Sci. Stat. Comput.* **12**, 631–644.

Vandewalle, N., Terwagne, D., Mulleners, K., Gilet, T. & Dorbolo, S. 2006 Dancing droplets onto liquid surfaces. *Phys. Fluids* **18**, 091106.

Welch, S. W. J. & Rachidi, T. 2002 Numerical computation of film boiling including conjugate heat transfer. *Numer. Heat Transfer* B **42**, 35–53.

Welch, S. W. J. & Wilson, J. 2000 A volume of fluid bases method for fluid flows with phase change. *J. Comput. Phys.* **160**, 662–682.

Youngs, D. L. 1982 Time-dependent multi-material flow with large fluid distortion. In *Numerical Methods for Fluid Dynamics* (ed. K. W. Morton & M. J. Baines), pp. 273–285. Academic Press.

Yue, P., Zhou, C. & Feng, J. J. 2006 A computational study of the coalescence between a drop and an interface in newtonian and viscoelastic fluids. *Phys. Fluids* **18**, 102102(1)–102102(14).

Zhang, F. H., Li, E. Q. & Thoroddsen, S. T. 2009 Satellite formation during coalescence of unequal size drops. *Phys. Rev.* L **102**, 104502(1)–104502(4).